Spray Pyrolytic Deposition of CdTe on Stainless Steel 304 Substrates

By Silas Kyalo Mathuku

Submitted in the Partial Fulfillment of the Requirements

for the Degree of

Master of Science

in the

Chemistry

Program

YOUNGSTOWN STATE UNIVERSITY

August 2023

Spray pyrolytic Deposition of CdTe on Stainless Steel 304 Substrates

Silas Kyalo Mathuku

I hereby release this thesis to the public. I understand that this thesis will be made available from the Ohio LINK ETD Center and the Maag Library Circulation Desk for public access. I also authorize the University or other individuals to make copies of this thesis as needed for scholarly research.

Signature:

_____

Silas Kyalo Mathuku, Student Date

Approvals:

_____

Dr. Clovis A. Linkous, Thesis Advisor Date

_____

Dr. Christopher Arntsen, Committee Member Date

_____

Dr. Allen D. Hunter, Committee Member Date

_____

Dr. Joe Simeonsson, Committee Member Date

_____

Dr. Salvatore A. Sanders, Dean of Graduate Studies Date

ABSTRACT

Today's society is mainly dependent on fossil energy sources despite being not sustainable, not renewable, and not environmentally friendly, as they generate a lot of carbon dioxide. Hydrogen is a promising substitute for fossil fuels. It is a clean fuel with water as the only oxidation product, thus less production of CO_2. Cadmium telluride (CdTe) is a promising semiconductor material that could facilitate the use of solar energy in producing hydrogen gas. CdTe can be a p-type photoelectrode that can perform electron transfer processes with an electrolyte. As a cathode, it reduces hydrogen ions in water to form hydrogen gas. Spray pyrolysis method, which is simple and easy to use, cheap compared to vacuum deposition methods, can produce uniform films over large surfaces within a short time, many small substrates at the same time, and whose concentration of precursor solution remains constant with time, was used in this project. CdTe films for this project were fabricated on stainless steel 304 substrates at different substrate temperatures and spray times. The precursor solution was based on a mixture of $CdCl_2$, TeO_2, hydrazine, and EDTA. Characterization of the fabricated films was done using X-ray diffraction, scanning electron microscopy and energy dispersive spectroscopy (SEM-EDS), stylus profilometry, cyclic voltammetry, and linear sweep voltammetry. The fabricated CdTe films had a uniform and highly crystalline surface morphology, that was Te-rich (p-type) and exhibited photoactivity with the evolution of hydrogen gas. The best photoelectrode was fabricated by spraying a mixture of equal volumes of 0.02 M solutions of Cd and Te salts onto a SS 304 substrate held at 330 ^oC for 3 min, which produced a 10 μm-thick film and a photocurrent of 5800 $\mu A/cm^2$ observed at -0.5 V. When a dispersion of Pt catalyst was reduced onto it, a photocurrent of 7700 $\mu A/cm^2$ was observed at -0.5 V, which compares well with other fabrication methods.

ACKNOWLEDGMENT

I would like to acknowledge several individuals who accorded me support in various ways in the process of working on this thesis. First and foremost, my sincere gratitude goes to my thesis advisor Dr. Clovis A. Linkous for his guidance, support, and academic advice during the whole process of identification, development, experimentation, presentation, and writing up of this thesis document. I am thankful to him for always being there, motivating and encouraging me in the many courses that he taught me and in this thesis. I would also like to thank Dr. Allen Hunter for his continued support from the courses he took me through for offering a lot of guidance during the undertaking of my thesis. My appreciation also goes to Dr. Arntsen Christopher for guiding me on the improvements I needed to do in the preparation of this document. Mya appreciation also goes to Dr. Simeonsson for his dedication, support, and for being part of my advisory committee. Special thanks go to Mr. Ray for assisting in the instrumentation processes.

I would also like to thank my family for standing with me during my study period. Special thanks go to my fellow graduate students Geoffrey, Moses, Samuel, and Onyinyechukwu for the help and cooperation they accorded me. You played a crucial role during the whole study process and especially during this thesis preparation. I would like to thank my friends for the various forms of support they accorded me.

Finally, I would like to thank the Chemistry department and the Youngstown State University fraternity for giving me this study opportunity that enabled me to reach this far.

TABLE OF CONTENTS

LIST OF TABLES

LIST OF FIGURES

CHAPTER 1: INTRODUCTION

1.1 World's energy situation

Energy is the ability to do work and we need the energy to execute day-to-day activities. Energy is essential to running all sectors of the economy ranging from production in industries, lighting, cooking, transportation industry, warming buildings, military, space exploration, and office equipment among other uses.

Despite the fact that energy is required in all sectors of modern life, the biggest percentage of the current energy sources is non-renewable and threatening to become depleted with time.[1]

Energy demand and consumption have tremendously increased in the last two centuries due to industrialization and modernization of human activities, putting pressure on the existing energy sources. Demand for energy continues to grow with a lot of pressure on energy sources as people become wealthier and populations continue to grow. As technology advances and people become more mobile with the adoption of modern life, nothing seems to go easy on energy demand. The growing energy demand coupled with limited technology to obtain energy completely from renewable sources have been an impediment in transitioning toward low-carbon sources and turning away from overreliance on fossil fuels.[2]

The graph below shows total global energy demand over time. It depicts the large increase in energy demands over a period of about two centuries with a worrying trend of overreliance on non-renewable energy sources. These non-renewable sources accounted for about 80% of the total energy sources in 2019.[3]

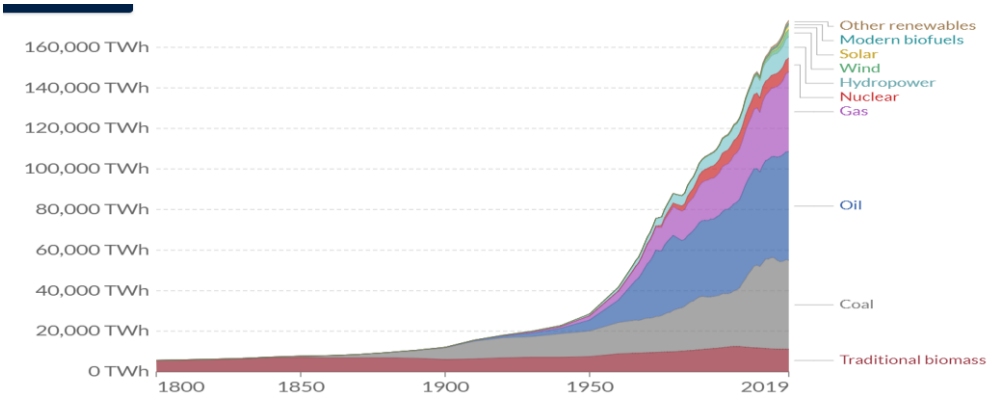

Figure 1: Energy demand and the different sources over the last two centuries.[2]

1.2 Non-renewable energy

The U.N arm on climatic change defines non-renewable energy as energy production from energy sources that are finite and hence cannot be replenished upon their exhaustion.[4] It is also defined as energy sources that will eventually run out with Nature having no capability to replenish them in the immediate near future or in our lifetime.

The non-renewable energy sources are mainly fossil-based fuels, which have carbon as the main element. These are fuels that formed many millions of years ago from dead plants and animals that trapped sunlight through photosynthesis before being buried. The main forms of these fossil fuels are coal, natural gas, and petroleum.

These energy sources have been very vital to human industrial development and advancement in technology and some of their advantages include: they are relatively inexpensive to extract, they can be easily handled, stored, and transported with little risk, they have a wide range of components that can easily be separated for different uses, and that they release high amount of energy upon their combustion and require relatively little technology to use.[4]

However, despite the versatility of these fuels in industrial development, their drawbacks stand out to challenge these advantages. Some of the challenges faced in using these fuels include: Fossil fuel sources are non-renewable and once depleted cannot be replenished in our lifetime. Another serious point of concern is that burning fossil fuels releases carbon dioxide into the atmosphere, which upsets the earth's carbon dioxide composition. Carbon dioxide occurs in the atmosphere naturally making about 0.04% of the atmospheric air. Additional release of carbon dioxide into the atmosphere has adverse effects, including global warming, which is the rise in the average temperature of the atmosphere. Carbon dioxide gas is a greenhouse gas that traps the sun's energy and retains it in the atmosphere. This greenhouse effect has led to catastrophic events including the melting of ancient glaciers leading to flooding in low-lying land masses, extra-ordinary heavy rains, and desertification.[4]

Figure 2 below shows the worrying trends of carbon dioxide increase in the atmosphere and the effect to the average global atmospheric temperature over time.

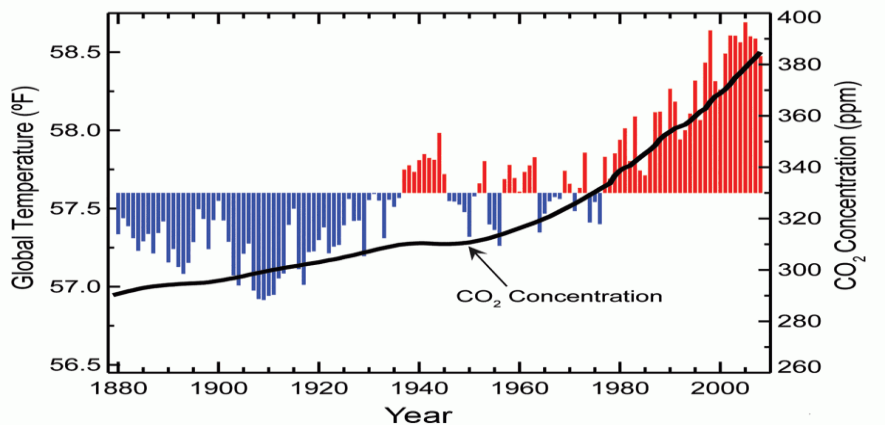

Figure 2: Trends in atmospheric carbon dioxide concentration and the effect on global temperature over the given period of time.[4]

Figure 2 above shows a dramatic increase in the atmospheric CO_2 concentration and especially from the 1960s. This can be attributed to advancements in technology where energy demands have increased. Many industries and the transportation sectors heavily rely on burning fossil fuels. Demand for electricity has also accelerated the burning of more fossil fuels to supply electricity for both domestic and industrial purposes.

Other non-renewable energy sources include:

Nuclear energy- This is the energy produced during nuclear fission in which the nucleus of certain atoms is split. Despite the fact that nuclear energy is considered quite renewable, the materials used in nuclear power plants are not renewable. Radioactive uranium isotopes used in nuclear plants are rare and their constant extractions spell doom for this type of energy. Also, the spent radioactive fuel is still quite active and must be isolated and protected for thousands of years.

Biomass- This type of energy comes from plant matter. Although plants can be grown, a delicate balance should be struck between their use and replenishment. If humans don't plant more, then this type of energy will definitely run out. In addition, there is a time-lapse between growing plants and harvesting.

These environmental concerns associated with non-renewable energy sources demand immediate actions to be taken to curb the destruction to the environment and ensure sufficient energy supply. Attention and a lot of effort need to be directed toward harnessing energy from renewable and sustainable energy sources.[4]

1.3 Renewable energy.

According to the United Nations climatic change action chapter, renewable energy is defined as energy that is derived from natural sources whose rate of replenishment is higher than the rate at which they are being consumed. In addition, these energy sources should be plentiful and easily available.[4] U.S office of energy efficiency and renewable energy, defines renewable energy as the energy that is produced from sources that are naturally replenished and do not run out. These energy sources include hydropower, solar energy, wind energy, geothermal power, energy from biomass, and tidal and wave power.

Some general benefits of using renewable energy sources in a country include: reliability and resilience of the natural grid system, offers employment opportunities, increase in the nation's energy independence, reduced carbon dioxide emissions, clean energy access to remote areas that are away from the traditional national grid system, and increased affordability of energy due to lower costs compared to non-renewable energy generated power.

In the USA, renewable energy constitutes only about 20% of all electricity demand, despite the obvious advantages of using renewable energy. Figure 3 below shows the percentage contribution of each renewable energy source towards this 20% in the year 2021.[4]

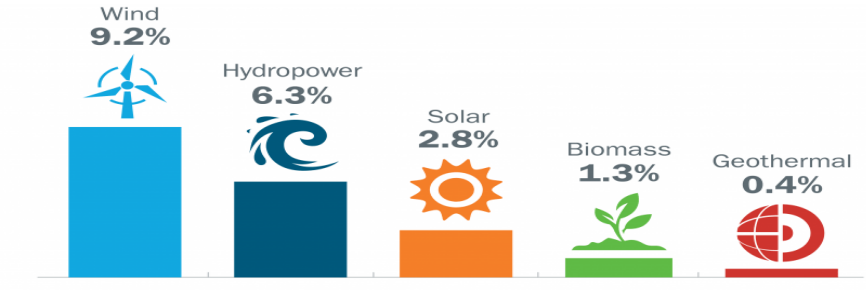

Figure 3: Renewable electrical energy use in USA by percentage of the total electricity use in year 2020.[4]

1.4 The sun as an energy source

The sun is a radiant source of energy. The energy in the sun comes from nuclear fusion that takes place like in any other star. Our sun is an average-sized star that is destined to continue supplying energy for the next 5 billion years. The sun releases an enormous amount of energy that drives almost all the earth's energy requirements. The sun's energy is used to keep the earth warm, drive the weather patterns, create sea and ocean currents, initiate wind, evaporate water in the oceans leading to rainfall, and is used by the green plants to make food through photosynthesis.

The sun is a typical black body radiator like any other star. Stars like the sun are perfect examples of black bodies which have a surface temperature pretty much higher than their surroundings and hence they emit electromagnetic radiation to their surroundings. The higher the temperature of the black body, the higher the intensity of the emitted radiation as described by Stefan-Boltzmann's law.[5]

Wien's displacement law postulates that increase in temperature of a black body leads to a decrease in the emitted wavelengths which implies an increase in the energy of the emitted radiation. For example, a body at room temperature emits radiation mainly in the infrared region.

The sun as a black body has a surface temperature of 5777 K. At this temperature, the sun emits most of the radiation at about 500 nm-800 nm which is mainly in the visible region, as shown by the band in Figure 4 below.

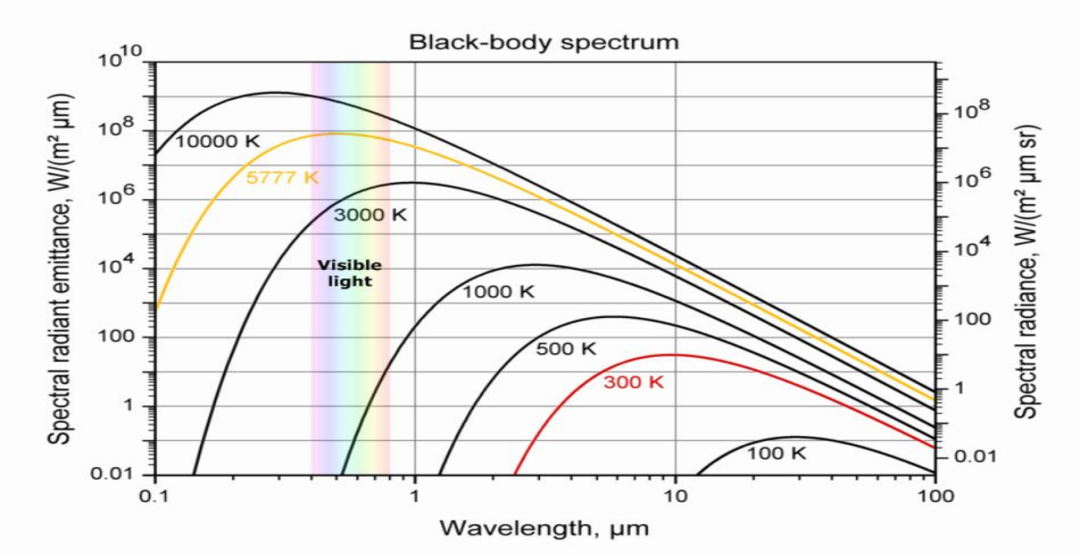

Figure 4: Black body radiation spectrum.[5]

On a bright sunny day, the sun's energy per square meter reaching the earth can power an average computer. This is usually about 1370 W/m^2. However, not all of the sun's energy incident on the earth is used, some is reflected back into the atmosphere.

This abundant solar energy could be harvested for use and serve as an alternative source of energy by converting it to electrical energy using photovoltaic cells. These cells are mounted to form solar panels, which can have a large surface area. The harvested solar energy can then be stored in chemical form in the different forms of storage that exist. This would ease the burden of overreliance on fossil fuels.

There are several advantages of using solar energy as outlined by Anaa.[6] These include:

- Solar energy is a clean form of energy and hence has little negative effects compared to fossil fuels.
- Solar energy is mostly quiet hence does not cause noise pollution compared to other sources like hydroelectric power and diesel generators.

- Use of solar energy helps to save water as almost no water is required compared to nuclear power sources that use enormous amounts of water.
- Installing solar panels helps to reduce monthly electricity bills.
- Solar energy has the advantage of reliability since the energy source is always there, it's free and available to all.
- Low maintenance costs- solar panels and devices require very little maintenance once installed and components can last for a very long time.

1.4.1 Challenges in harvesting solar energy

Despite the many advantages, solar harvesting has yet to be fully embraced. The challenges that face solar energy harvesting include.

- Low solar panel efficiency. Despite abundant free solar energy, only a small percentage can be converted to electrical energy by solar panels.
- Initial costs for installing solar panels and solar equipment are quite high and require a good input of capital.
- Scarcity of materials for PV cells.
- Seasonal variations of solar insolation.[6]

Sustainable and renewable energy sources are a promising solution to environmental concerns. The major challenge of harnessing sources of energy, especially solar energy has been the storage of the energy since the sun is only available during the day and there exist very large seasonal variations in solar insolation.

Different types of batteries may be used for the storage of solar energy. These batteries are mainly charged during the day when the sun is shining and then used when the sun goes down.

Despite their practicality, battery capacities are limited, and tend to lose their capacities with time. They also drain quickly, hence may not provide enough energy for long. This calls for a look into a better method of storing the sun's energy.

1.5 Hydrogen as an energy carrier

Hydrogen is not a source of energy but is an energy carrier that can be used to store harvested solar energy. Kasper (2017), described hydrogen as a potential solution to the storage of energy harvested from the sun. Hydrogen is a gas at ambient conditions and therefore reasonable storage can be achieved by storing it in compressed tanks or in adsorbed states. They outlined the advantages possessed by hydrogen as a fuel. One of them is high elemental abundance; hydrogen is the most abundant element in the universe and accounts for about 15 mol% of the surface of the earth. Hydrogen is a clean fuel and when consumed gives water as the only byproduct. It is also easier to recharge hydrogen fuel sources than battery-based storage. Another very important aspect of hydrogen is that hydrogen has the highest gravimetric density (energy density) value of 286 kJ/mol or 51920 Btu/lb or 143,000 KJ/kg. Finally, hydrogen can be combusted or used in electrochemical cells directly to produce electricity.[7]

Even though solar power energy is a promising and free source of sustainable renewable energy, it only contributes to a mere 20% of the total electricity used globally with fossil-based sources still dominating. This, therefore, calls for more investment in research work towards producing more competitive systems and technologies for harvesting this clean solar energy and hence reducing environmental pollution which arises from burning fossil-based fuels.

CHAPTER 2: LITERATURE REVIEW

2.1 Photovoltaic cells

The photovoltaic cell (solar cell) is a device that uses photons or light particles to generate electricity by a process called the photovoltaic effect. The photovoltaic effect was discovered by French scientist Edmund Becquerel in 1839. He made the first PV cell when he was only 19 years of age. He used silver chloride which he placed in an acidic solution and then shone a light on it while connected to platinum electrodes. By this, he generated a current and a voltage.[8]

In 1876, an English engineer, Willoughby Smith, discovered the photoactivity of selenium. Three years later, Grylls Adams and Richard Day proved that electricity could be generated from selenium just by the use of light and not necessarily heat or moving parts. In 1883, New York inventor Charles Fritts created the first real solar cell. He made the cell by coating selenium with a thin layer of gold. His cell had a maximum cell efficiency of 2%.[9]

In the year 1887, Heinrich Hertz discovered the photoelectric effect. This is the phenomenon by which electrons are ejected from a metal surface when radiation of sufficient energy falls on the metal. He discovered that ultraviolet radiation caused a greater photoelectric effect compared to red and green radiation regardless of their intensities. Albert Einstein further explained this photoelectric effect mathematically and won a Nobel prize for it. He explained that light travels in discrete packets called photons. The energy, E, of a photon, is proportional to the frequency, f, of the radiation and is given by:

$\mathbf{E = hf = hc/\lambda}$ where h is Plank's constant, c is the speed of light, and λ is the wavelength of the incident radiation.

This explains the differences in energy as observed in photoelectric effect.

In 1956, the first practical solar cell made from silicon was fabricated by Bell Laboratories. This came after the discovery that silicon had a higher efficiency than selenium. With an efficiency of 6%, the silicon cell could power electrical equipment. Using silicon-based solar technology, the first solar-powered satellite was put into orbit in 1958. In the 1960s solar cells were put into more use when they found use in space exploration vehicles and satellites. However, the cost of production of solar cells was very high and, thus their use was only limited to government agencies like NASA. The first solar park was built in 1982 in Hesperia California which generated 1 MW when in full operation. Later, another park was built in the Carrizo plains in California and had a capacity of 5 MW.[9] Now there are several solar farms whose capacity exceeds 300 MW.[10]

The rising costs of fossil fuels and the need for clean cheaper energy would spark governments in different countries to invest in solar technology, which received lucrative incentives to adopt it. Further applications and commercialization for domestic and other large-scale use would continue into the late 1980s. However, the 21st century has seen tremendous changes in the development and utilization of the photovoltaic effect with many photovoltaic cell manufacturing companies coming into being. Many nations have also significantly adopted solar technologies with the ultimate goal to reduce overreliance on fossil-based fuels and also with a view to reducing global carbon dioxide emissions.

2.2 Working principle of PV cells

2.2.1 Fermi energy and Semiconductors

Fermi energy is the measure of the energy of the least tightly held electrons within a solid or simply the difference in energy between the highest and the lowest occupied states. Fermi level refers to the highest energy level that an electron can occupy at an absolute zero temperature. At the absolute zero temperature, the Fermi energy level lies between the valence band and the conduction band, which is in the middle of the energy band gap in the semiconductors as shown in Figure 5 below.

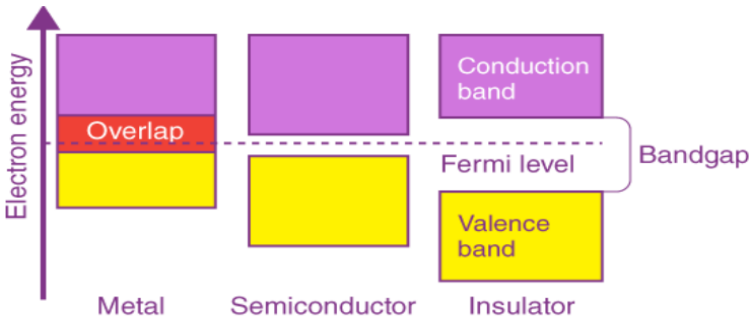

Figure 5: Fermi energy and band gap for metal (conductor), semiconductor, and insulator.[11]

When the temperatures are increased, the Fermi level stays constant while some of the electrons go to higher energy levels. In the case of semiconductors, the electrons go to the conduction band. In insulators, the energy band gap is too large for electrons to move to the conduction band. Fermi energy is very useful in describing conductors, semiconductors, and insulators. Understanding Fermi level and Fermi energy concepts is very important in designing semiconductors. The Fermi level is usually slightly below the conduction band in an n-type and just slightly above the valence band in a p-type semiconductor. The Fermi level of

semiconductors can be varied by changing the conditions of temperature or input of any other form of energy that excites electrons. When p-type and n-type semiconductors are joined together, the Fermi energy level for the n-type decreases while that of the p-type increases until equilibrium is achieved.[11]

The Pauli exclusion principle dictates that each energy level can be occupied by no more than two electrons with two opposite spins. The probability of electrons occupying a given energy level is given by the Fermi-Dirac distribution function below. At a given energy E, the number of states that may exist is found from the density of states. The number of states of energy that will be filled by electrons is specified by the Fermi function *f*(E).

$$f(E) = \frac{1}{1 + e^{(E-Ef)/KT}}$$

where E is the energy, E_F is the Fermi level, K is Boltzmann's constant = 1.38 x 10^{-23} J/K, and T is the absolute temperature.

As the temperature increases, the probability of the electron moving to higher energy states increases. At the absolute zero temperature, *f* (E) is 1, implying that all the electrons are below the fermi level.[11] This is important in understanding semiconductors that depend on external energy to boost their conductivity hence their conductivity can be controlled to suit certain functions.

2.2.2 Semiconductors

These are materials that have their conductivities between that of conductors and insulators. Germanium and silicon are examples of pure semiconductors called intrinsic semiconductors. Semiconductors can also be extrinsic meaning that they are not pure. This is achieved by doping

with suitable dopants. In semiconductors, the electrons and holes are the charge carriers. The holes are positive while the electrons are negative. However, electron experience higher mobility than holes since the holes experience more attractive force from the nucleus than the electrons. For example, at 300 K, electrons in Si have mobility of 1500 $cm^2(V.S)^{-1}$ while that of the holes is 475 $cm^2(V.S)^{-1}$. Electrons usually travel within the conduction band while the holes in the valence band.[26]

The energy band theory discovered by Walter Heitler and Fritz London brought an understanding of conductors, semiconductors, and insulators at microscopic levels as explained in the energy band theories.[12,13] In solid lattices, energy levels are split into energy bands. This leads to the creation of two bands which are the conduction band and the valence band.

Valence band- this is the highest occupied energy level. It always contains electrons.

Conduction band- the lowest unoccupied energy level. It is a high energy level that is mostly devoid of electrons.

The band gap- this is the gap between the valence band and the conduction band.

For conductors, both the valence band and the conduction bands overlap. This makes the electrons to be always available in the conduction band hence conductivity in all conditions.

In semiconductors, the energy band gap is smaller than that of the insulators. Electrons can be promoted from the valence band to the conduction band by varying the conditions of temperature. This makes the conductivity of semiconductors improve with an increase in temperature.

In insulators, the energy band gap is too wide even with an increase in temperature, no electrons can occupy the conduction band hence their conductivity is not affected by temperature.[13,14] The relative band gaps are shown in Figure 6 below.

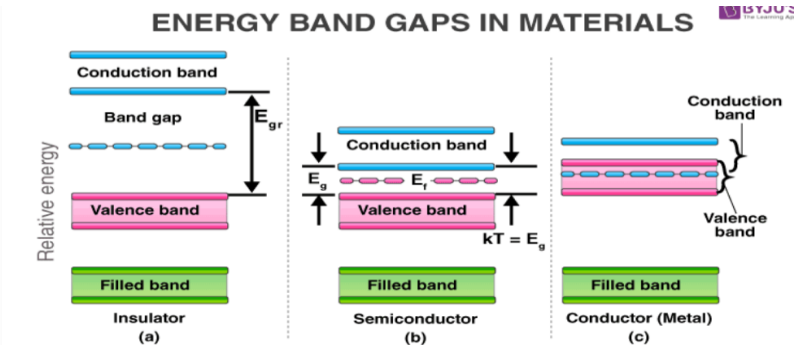

Figure 6: Relative energy band gaps for insulators, semiconductors, and conductors.[13]

The intermediate electrical conductivity property of semiconductors makes them good candidate materials for tunable electrically conductive devices. As earlier stated, electrons can be promoted from the valence band to the conduction band thermally or by the use of light energy.

Intrinsic semiconductors are completely insulators at absolute zero temperatures. An increase in temperature causes some of the bonded electrons to be free to move leaving behind holes.

Extrinsic semiconductors are impure due to doping. In the doping process, one of the lattice atoms of the intrinsic semiconductor is replaced by a dopant atom. Doping can give rise to either of the two types; the n-type and the p-type.

N-type is created by doping an intrinsic semiconductor with an element containing excess valence electrons. Some of the electrons bond covalently in the structure while the excess electrons are left free. These free electrons contribute to the increase in negative charge carriers. In this way, the electrons become the majority charge carriers while the holes become the minority charge carriers.

P-type doping occurs when an intrinsic semiconductor is doped with atoms containing a deficit of valence electrons. During the bonding process, there is a deficiency of electrons, leaving a positive “hole”. This increases the number of holes in the semiconductor resulting in p-type conductivity. The positively charged holes become the majority charge carriers while the electrons become the minority charge carriers.

In the fabrication of cadmium telluride thin-film PV cells, the stoichiometry is arranged so that there is a deficiency in cadmium during the crystal lattice formation with tellurium. The cadmium vacancies trap electrons leading to an excess of free positive charges on p-type semiconductors.[13,14]

The materials making PV cells absorb the energy of the photons falling on them from the sun. This generates electrons that are free to move within the material. The release of these electrons leaves vacant positions called holes. To force the electrons to flow in one direction, PV cells are made of two main layers. In a Si-based cell, one side is made of silicon doped with phosphorus. This creates an excess of electrons in the overall structure and this side becomes the positive terminal called the n-type however it remains neutral until it is contacted by the p-type phase.

The other side consists of silicon doped with boron, a trivalent element. The bonding of boron with silicon creates a deficiency of electrons called holes and this side is called p-type. The two types of layers can be brought together to form what is called the p-n junction, facilitated by the diffusion of electrons and holes in the opposite direction.

When light of sufficient energy (higher energy than the energy binding the valence electrons) falls on the semiconductor, electrons absorb the photon energy and flow to the n-type side, while

the holes flow towards the p-type side mobilized by the electric field. When the two sides are connected externally, direct current flows.[15]

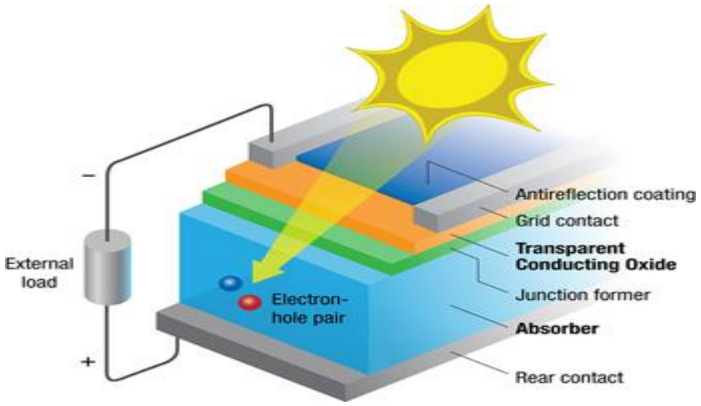

Figure 7: An illustration of a solar cell.[15]

2.2.3 Solar panels efficiency

Of all the renewable energy sources, solar energy stands out as the most attractive source of energy which is very promising and has drawn a lot of attention due to its abundance, being free and readily available, and being a totally renewable resource. However, harvesting solar energy for electrical energy has been a challenge due to solar panels' efficiency.

On the earth's surface, the earth receives about 1374.7 W/m^2. However, only a small fraction of this energy can be harvested by PV solar panels. This is due to limitations on the solar panels in that only one electron can be excited by one photon regardless of the photon energy. The PV solar cell's limitation of maximum efficiency is called the Shockley-Queisser limit.[16]

2.3 Leading types of PV cells

PV cells can be classified into 3 categories based on their generations.

Silicon cells- The silicon-based PV cells are the oldest. They are also currently the dominating solar module in the PV solar panel market for providing substantial electrical power and collecting sunlight over large areas. There are two types of silicon-based PV cells.

2.3.1 Polycrystalline silicon solar panels

These are also called polysilicon. Produced using the Siemens process, which involves the distillation of volatile silicon compounds and the eventual decomposition of the compounds to obtain pure silicon. The silicon ingots are then cut into thin wafers. Polycrystalline silicon consists of different grains/crystals of silicon in different orientations. These crystals cause this type to have a characteristic blue metal flakes appearance as shown in Figure 11. The surface of polycrystalline silicon is thus less perfect due to the many crystals with different orientations, which is responsible for little absorption of solar energy compared to monocrystalline forms.[17]

One square meter of polycrystalline silicon cells generates about 175 W.

Figure 8: Polycrystalline silicon[17]

2.3.2 Monocrystalline silicon solar panels

Monocrystalline solar cells are made from pure silicon ingots made from a single crystal. The process of making monocrystalline silicon begins with a pure silicon seed crystal. The seed is placed in a large vat full of molten silicon and slowly drawn with silicon slowly forming around

it. This produces a large ingot which is then cut into wafers. These wafers are then mounted to form a single solar panel which consists of 60 or 72 wafers per solar panel.[18]

Figure 9: A monocrystalline silicon solar panel.[18]

Table I: Some comparisons between polycrystalline and monocrystalline silicon cells.[18]

Property	**Polycrystalline**	**Monocrystalline**
Color	Blue flaky appearance	Black color
Watts /m^2	175	190
Lifespan	25 years	35 years
Cost	Cheaper	Quite expensive
Efficiency	15-18%	18-25%
Effect of temperatures	Adversely affected by high temperatures	Does well in conditions of high temperature and dim light

2.4 Shockley-Queisser limit

This is the amount of electrical energy that a solar cell can extract from an incident photon. It's the upper limit for a single junction that uses an absorber material with a specific band gap. The

theoretical efficiency of solar absorption has currently been calculated as 33.7% at 1.34 eV. It's this limit that the fundamentals of solar energy production with photovoltaic cells are based.[19,20]. A plot of maximum obtainable efficiency versus band gap energy is shown in Figure 9. It is seen that Si despite its prominence as a PV material is well off the maximum in the curve. On the other hand, GaAs and CdTe have band gaps at 1.42 and 1.44, respectively which are nearly exactly at the peak of the curve.

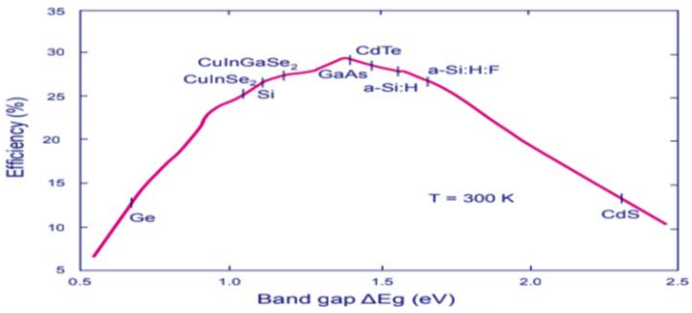

Figure 10: The Shockley-Queisser limit [19]

2.5 Thin film PV cells

These PV cells also make use of single-junction devices and are manufactured using thin film technology. In this technology, materials are deposited on the surface of a substrate, which may be glass, plastic, or metal. Since they use very little material, their cost of production is greatly reduced. This technology uses a variety of methods for deposition like electrodeposition, solution bath method (electroless method), sputtering, and spray pyrolysis. In this category, the main types of cells are:

- The amorphous silicon
- Cadmium telluride, copper indium gallium selenide, gallium arsenide.[21]

This 2nd generation of solar PV cells has currently a market share of about 20% which is mainly due to CdTe. Due to the few semiconductor materials used, their efficiency is quite low. Some of the second-generation PV cells and their properties are as below.[21]

Table II: Some 2nd generation PV cells and their properties

Type	Efficiency	Advantages	Disadvantages
Amorphous silicon (a-Si)	4%-8% in market Max. lab efficiency at 12%	The cheapest in the market	Very low efficiency due to the amorphous nature of the semiconductor material used
GaAs	Max. lab efficiency at 29% The band gap of 1.43 eV	High efficiency Less bulky	High cost
CdTe	10%- 15% efficiency Max. lab efficiency at 21% Band gap of 1.45 eV	CdTe exploits a broader wavelength of the spectrum than the silicon cells. Low cost	Cadmium is very toxic
CIGS	Has a max. efficiency at 20% Has a band gap of 1.68 Ev.	Less intensive process than in si-based cells Good resistance to heat.	Very expensive to produce Uses toxic materials to produce.

2.6 Working of thin film PV cells

Thin films consist of a semiconductor material deposited on a suitable substrate or can be defined as a material created by random nucleation and growth of individually condensing/reacting atomic /ionic or molecular species on a substrate. These materials are usually a few microns in thickness and are able to absorb the sun's radiation and convert it to electrical energy. Cadmium telluride thin-film cells are the most common in this category because they are relatively cheap to produce than other thin cells.[22]

2.7 CdTe photovoltaics

These are thin film PV cells based on cadmium telluride, which work by absorbing sunlight and converting it to electrical energy. CdTe thin film technology has been cited as one with the lowest production costs and the least payback time of less than a year. Additionally, this technology has been shown to have the lowest carbon footprint. Cadmium is itself a cheap material that is a byproduct of mining zinc and hence its production is not tied to the manufacturing of PV cells. On the other hand, tellurium is a quite rare metal and contributes significantly to the overall cost of the PV module.

A significant challenge that is associated with CdTe thin films is the toxicity of cadmium associated with the production and disposal of CdTe solar materials. However, CdTe is a very stable substance, and once sealed off, it will never come out to interact with the environment. Furthermore, the lifespan of these films is about 35 years and methods have been devised to recycle the cadmium telluride.[22]

2.8 The design of a functional CdTe PV cell

A CdTe cell has CdTe as the main light absorber. In the setup, p-type CdTe is matched with n-type CdS. To facilitate the movement of higher currents across the top of the cell, transparent conducting oxide (TCO) such as tin oxide is used instead of a metal grid.[23]

Most recent advancements in design have seen the efficiency of CdTe thin films at 22.1% as announced by the First Solar company in 2016. Some of the measures employed to maximize efficiency have been alloying, which helps in broadening band gap grading and improving quantum efficiency response for a wider range of wavelengths. Selenium has been incorporated into the manufacture of CdTe films which has seen an improvement in efficiency. Magnesium zinc oxide (MgZnO) has also been incorporated instead of CdS to improve efficiency because it has a tunable band gap and can be optimized for high performance.[23,24]

2.9 Why thin-film PV materials are of interest

Photovoltaic materials are inorganic semiconductors that form junctions with other materials and exhibit the photovoltaic effect when exposed to light. The most ideal PV materials for solar absorption should have a band gap of about 1.5 eV and a solar absorption of about 10^5/cm. A good PV material should also have high quantum efficiency for charge carrier generation and, should be able to form a good electronic junction with a suitable material. The optical absorption of a solar cell is the inverse of the optimum thickness implying that the thinner the film, the higher should be the absorptivity.

Elemental materials are seemingly the best from the point of manufacturing thin film PV cells. However, it is unfortunate that there is no elemental material that has a band gap of 1.5 eV. Silicon, an elemental PV material has a band gap of 1.1 eV. To have reasonable absorption, a

minimum thickness of 50 microns will be required. Years of continued research have led to the fabrication of a metastable alloy film of a-Si:H. This material has a band gap that can be tailored, is easily doped and with a reasonably high optical absorption coefficient.

Other than a-Si:H alloy, other binary materials which show promising PV activity include: GaAs, CdTe, Cu_2S, Cu_2O, InP, Zn_3P. From this list, GaAs and InP are the most ideal for PV activity with a band gap of 1.42 eV. However, these materials are too expensive for making commercially viable solar cells.

A practical solar cell contains a junction made by placing two dissimilar materials together and creating an electronic barrier that separates the charges. For a solar device to be efficient, it must have a high conversion of photo-energy and also have a good collection efficiency for the excited charge carriers. Many junction devices with appropriate band gaps may be integrated or placed in tandem to form multi-junction. However, the question then is, how many junctions may be employed and what is the maximum achievable efficiency? Theoretically, it has been calculated that an efficiency of about 53% can be achieved with four-junction devices. As the number approaches infinity, the theoretical efficiency reaches 68%. However, the complexity of matching such junctions has limited this to only three junctions.[25]

Sources site CdTe as an ideal absorber material for fabricating high-efficiency, low-cost thin-film polycrystalline cells. The reason for so much attention on CdTe is that it has almost an optimum energy band gap for solar absorption. CdTe has a direct band gap of about 1.5 eV and an absorption coefficient of 10^5/cm in the visible spectrum. This means that a film of only a few microns is required for the absorption of about 90% of the incident photons.[25,26,27]

Fabrication of cadmium telluride films is often in such a manner that the deposition has a deficiency of cadmium, giving rise to a p-type semiconductor. The CdTe solar cell uses the p-n junction format. The arrangement of the components is usually in the following order: on the surface is the glass substrate, which is transparent and allows light through. A transparent conducting oxide (TCO) is the next. In most cases, indium tin oxide (ITO) is used. However, zinc oxide is also a preferred TCO due to its superior qualities of high transparency to visible light and is very stable up to 800 K. The next layer is the n-type layer. CdS is usually used as the n-type layer. In the CdTe (111) lattice plane and CdS (001), there is a mismatch of 9.7%. However, CdS still is the most effective heterojunction match for CdTe. The role the mismatch may play in such microscopic dimensions in polycrystalline films is not significant. The n-type is then in contact with the p-type CdTe which acts as the light absorber layer. The back contact is usually a metal or a metal alloy with a p-type conductivity and is required to have a work function greater than that of cadmium telluride.[27]

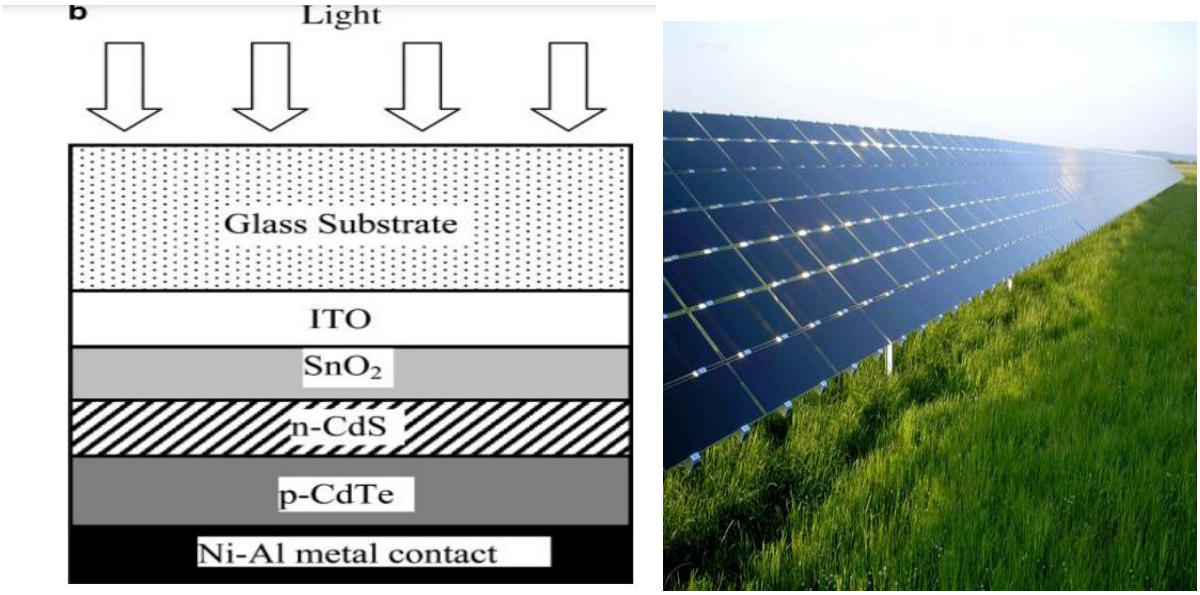

(a) (b)

Figure 11: (a) The design of a functional CdTe PV cell, (b) CdTe solar panels[27]

2.10 Cadmium telluride deposition methods

Several methods for cadmium telluride deposition exist. These include the electroless (chemical bath) method, electrodeposition method, successive ionic layer adsorption and reaction method (SILAR), spray pyrolysis method, pulsed laser method, molecular beam epitaxy, vacuum evaporation, sputtering, physical vapor deposition, and thermal evaporation.[28]

In this project, the chemical spray pyrolysis method is employed. The spray pyrolysis method involves spraying a metal salt solution on a heated substrate and a reaction taking place spontaneously to coat the substrate with the anticipated material.[28]

This method has extensively been discussed by various researchers and most have found it to have great advantages over other methods of deposition. Some of the advantages that have been cited include that the spray pyrolysis method is simple to undertake, it does not require high-quality substrates and chemicals, can produce films that are very even, it is possible to adjust the settings to vary the morphology, and the apparatus is simple and easy for large scale production. Also, there are no restrictions on the dimensions and the material.[29]

Literature exists on the use of the spray pyrolysis method for the deposition of cadmium telluride for photoelectrochemical activities. K.V. Krishna & V. Dutta (2003), have discussed the spray pyrolysis method at length. They were able to deposit CdTe films on glass substrates using $CdCl_2$ and TeO_2 both in 0.02 M concentrations with hydrazine as the reducing agent to obtain Te^{2-} from Te^{4+}. EDTA was also used as a complexing agent to delay Cd^{2+} release and

hence grow a Te-rich film. The temperature of the glass substrate was maintained at 400 ^{o}C, and so no annealing was done in their experiment though. They discussed the effect of the concentration of EDTA on the quality of CdTe films, with the conclusion that high

concentrations favored better crystalline films. However, they did not state or postulate how far this concentration of EDTA can go and the stoichiometry effect. Generally, they reported producing well-defined polycrystalline CdTe films and tests showing photoelectrochemical activity.[30]

Temburkar also reported using the spray pyrolysis method to deposit CdTe on a glass substrate using an aqueous solution of $CdCl_2$ and tellurium tetrachloride, each at 0.02 M concentration and maintaining the substrate at 350 ^oC and annealed the films at 400 ^oC for one hour. They reported photoactivity and a good morphology of the films showing polycrystalline CdTe films fabricated successfully.[31]

In the cases of spray pyrolysis discussed, it has been shown that this method was successful in all cases and the desired films were obtained. From the research done, it seems that the majority are depositing the films at 350 ^oC and annealing at 400 ^oC. However, there seems to be a discrepancy on whether to use a complexing agent or not and if the use of higher temperatures for spray pyrolysis rules out the importance of annealing the films later.

Dainius and Ludwig have discussed extensively the influence of different spray parameters on the quality of the films fabricated.[32] From their discussion, temperature seemed to have the biggest hand in influencing the properties of the thin films formed. Temperatures influence the way the atoms interact and the formation of crystals at very low-temperature leads to less evaporation of the volatile substances that are expected to leave. This leads to the formation of amorphous deposits and negatively affects the films. They also indicated that very high temperatures lead to the formation of pinholes hence optimum temperatures are required. However, they did not conclusively state the optimum temperature for spray pyrolysis, leaving it to experimental speculation. The precursor solution was also discussed as another important

factor that influences the quality of the films in spray pyrolysis and this factor influences greatly the morphology of the films. The concentration of the precursor solutions and the use of additives were cited as the biggest players in this case. Complexing agents could influence the elemental stoichiometry in the films.[32]

From the research articles listed, it is clear that spray pyrolysis has been used for depositing CdTe films for quite a while, giving positive results, and that several factors may affect the quality of the fabricated films. However, none of these reports have explored depositing CdTe films using the spray pyrolysis method on stainless steel 304 substrates. This project, therefore, aims to explore the viability of the spray pyrolysis method on stainless steel 304 substrates as compared to glass substrates used by other researchers.

2.11 Water splitting to produce hydrogen

This is the conversion of water into its elemental forms (hydrogen and oxygen). This process produces more pure hydrogen compared to other processes and especially producing hydrogen from fossil fuels. Electrolysis is a method of producing electricity but its run by electricity which is mainly from burning fossil fuels producing more CO_2 hence no point in reducing CO_2 emissions.[33]

For decades hydrogen production from the water-splitting process (photo-electrolysis) has been of interest and various methods of production have been put in place. Hydrogen is a very promising method of energy and by far can store more energy compared to battery-based energy storage systems. Hydrogen has a very high gravimetric energy density as a highly clean and sustainable energy carrier. When used in a hydrogen fuel cell, it has a higher energy conversion and emits water as the only byproduct.[33,34]

Research has been done and is still being done on the different effective and environmentally friendly water-splitting techniques to obtain hydrogen. The use of photoelectrochemical semiconductors for water splitting has been shown to be an alternative cleaner way to facilitate water splitting. In this system, a semiconductor plays the role of absorbing and using the sun's energy to split water to produce hydrogen.[35]

There are two redox reactions in the electrolyte. Upon absorption of light and generation of electrons and hole pairs, one redox system reacts with the electrons and the other with the hole pairs. Under the irradiation of energy higher than the energy band gap (E_{BG}), the electrons are excited to the conduction band (CB) and holes are generated at VB. The electrons and holes (which have not undergone recombination) move to the surface of the semiconductor and then reduce/oxidize molecules of water adsorbed on the surface. This leads to the production of hydrogen and oxygen at the cathode and the anode respectively.[35,36]

At the cathode $4H^+ + 4e \longrightarrow 2H_2$ $\Delta E^0 = -0.41$ V ---------- (i)

At the anode $2H_2O \longrightarrow O_2 + 4H^+ + 4e$ $\Delta E^0 = +0.82$ V----------(ii)

Overall equation $2H_2O \longrightarrow 2H_2 + O_2$ $\Delta E^0 = +1.23$ V----------(iii)

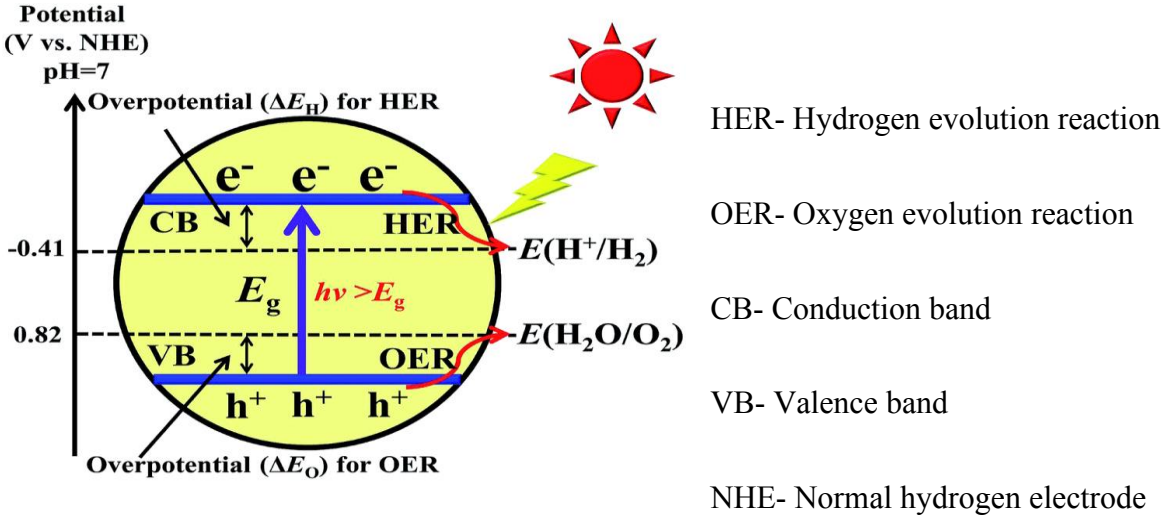

Figure 12: Diagram showing photoelectrochemical water splitting.[36]

This project, therefore, focuses on the fabrication of cadmium telluride materials on stainless steel 304 substrates for water splitting to generate hydrogen gas.

2.12 Cadmium telluride photoelectrochemistry: Why use cadmium telluride?

Many sources have indicated cadmium telluride as a promising versatile substance for water splitting to produce hydrogen. It is a promising photovoltaic material because it has an optimum band gap for the sunlight of 1.45 eV compared with the traditional silicon-based photovoltaic activity with a bandgap of 1.1 eV. CdTe also has a high solar absorption coefficient of 10^5 cm^{-1} and absorbs 90% of visible light in a thickness of just a few microns. Si requires 200 µm for such absorption. This means that cadmium telluride converts radiation energy even in lower or diffuse sunlight environments in comparison with the lower bandgap materials hence has more effective conversion and is suitable even for less sunny days or in cloudy weather. CdTe is also very stable

and can withstand adverse conditions and CdTe thin films are also more economical than traditional silicon-based solar cells.[37,38]

Cadmium telluride for water splitting to produce hydrogen is grown off-stoichiometric phase leading to a tellurium-rich environment that produces a p-type semiconductor.[38]

This project, therefore, focuses on the fabrication of cadmium telluride materials on steel substrate for water splitting to generate hydrogen gas. Naser Ali et al., (2019) have discussed extensively the properties of steel that make it suitable for the deposition of thin films and characterized stainless steel as a passive substance that is resistant to corrosion, strong and resistant to shattering, and has good thermal distribution due to its good thermal conductivity, and being an electrical conductor, it improves electrical contact in the films.[39]

2.13 The Pourbaix diagram and CdTe aqueous system

A Pourbaix diagram is a plot of potential E (V) against pH used in electrochemistry and corrosion science involving solutions and represents the thermodynamic stability of the aqueous electrochemical system. In this project, the analysis of the CdTe Pourbaix diagram has enabled the determination of the pH values where the precursor solution for spray pyrolysis of CdTe is most appropriate to avoid precipitation and have maximum solubility. At pH 11.5 and a potential of 0.0 V, the cadmium and tellurium ions are in solution and the solution is colorless and clear. The stability of the fabricated CdTe film is shown to be stable between lines 1 and 2 over the whole range of pH as shown in Figure 19 below. CdTe is also shown to be stable in the negative potentials to about -1.5 V. However, CdTe is very unstable at positive potential values. This then allows one to work within the limits of the voltage when carrying out photoelectrochemical analysis of the fabricated films. Sweeping to the positive voltage or too far to the negative (past -

1.5 V) would cause chemical etching of the films. The Pourbaix diagram also shows equilibrium lines for water reduction to hydrogen gas (line 3) and oxidation of H^+ to water (line 4).[40]

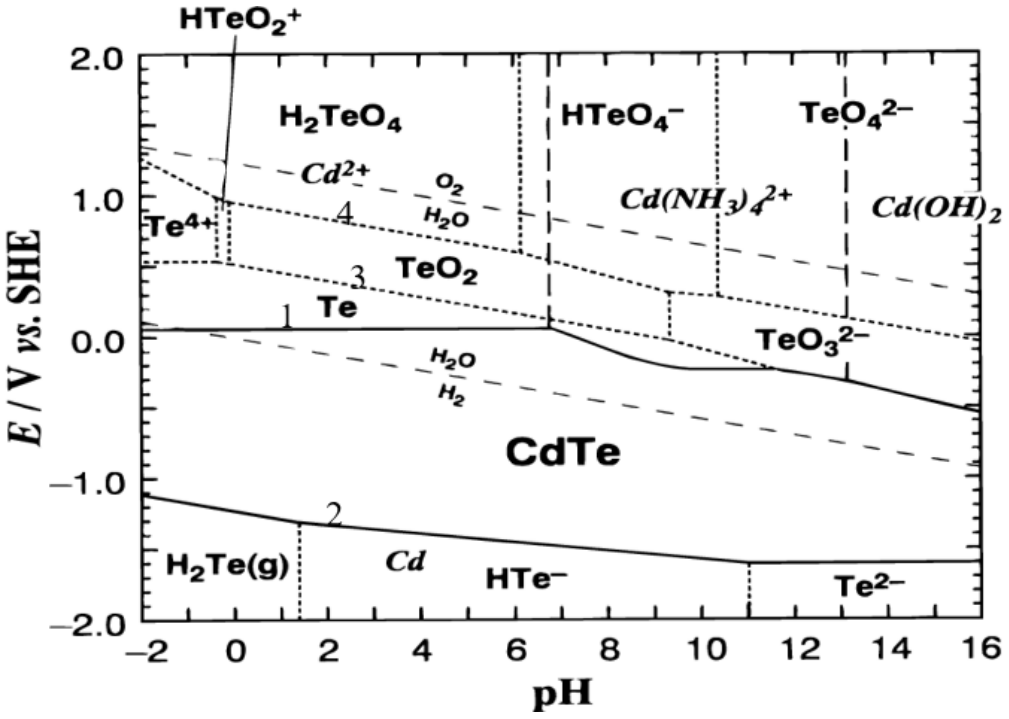

Figure 13: Pourbaix diagram for CdTe aqueous system at different pH values.[40]

2.14 Question to be answered

Is it possible to deposit a uniform CdTe film over a large area inexpensively and on a strong and cheap substrate such as stainless-steel 304 and use it as the active electrode to split water to generate hydrogen?

To answer the question, I have performed chemical spray pyrolysis of CdTe on steel substrate and carried out several analyses on the deposited material. In this project, the chemical spray pyrolysis method was done using a 3D printer. In spray pyrolysis, a metal salt solution (precursor solution) is sprayed onto a heated substrate with the reaction taking place spontaneously to coat the substrate with the anticipated material. This method has advantages over other methods in

that it is simple to undertake, may not necessarily use substrates of high quality or high-quality materials, can produce films that are very even, allows for adjustment of the settings to vary the morphology, utilizes simple apparatus easy for large scale production, and there are also no restrictions on the dimensions and the material to use.[41,42,43]

2.15 Significance of the study

A lot of interest has been shown in harvesting sunlight as a source of energy as a mitigation for the continued environmental pollution from burning fossil fuels. Upon realizing the important role thin-film solar PV cells can play in this task, I embarked to research more on the fabrication of cadmium telluride thin films for photoelectrochemistry in water splitting to produce hydrogen gas that can be used as a fuel. This research seeks to produce more uniform thin PV films on stainless-steel 304, which is a very versatile material. It is part of the continuation of CdTe work done in the lab which was initially done by Patrick Rutto in 2018, where he used the electrodeposition method [44], and later done by James Malika in 2020 where he used the chemical bath method.[45] However, upon revisiting their procedure, I found the issue of uniformity of their films in which most of the films were not very uniform. The two methods were quite involving and require a constant change of solutions as the concentrations of the solutions were varying with time. It was also a challenge to deposit over a large area. By using the spray pyrolysis method, this research project sought to deposit cadmium telluride on stainless steel substrates with intention of producing more uniform films continuously over large surfaces.

CHAPTER 3: METHODOLOGY

The objective of this project is to fabricate cadmium telluride thin films for water splitting to produce hydrogen gas. Out of the many possible methods for depositing CdTe thin films on a steel substrate, spray pyrolysis was the method applied in this research with a detailed procedure described in this chapter. The fabricated films were also characterized using different techniques which are: XRF, XRD, scanning electron microscope (SEM) studies, profilometry analysis, and finally photo-electrochemistry studies using cyclic and linear sweep voltammetry.

This chapter, therefore, focuses on the actual procedures involved in the production and characterization of the CdTe thin films.

3.1 Materials required

Distilled water, ammonium hydroxide (NH_4OH), hydrazine hydrate ($N_2H_4 \cdot H_2O$), hydrochloric acid (HCl), cadmium chloride ($CdCl_2$), tellurium dioxide (TeO_2), and ethylene-diamine-tetra acetic-acid (EDTA), platinic chloride salt, stainless steel plates (4cm by 3cm), and an INVENTOR3D spraying machine, thermocouple, heater oven for annealing, and cadmium sulfate.

All the chemicals and apparatus used in this research experiment were already available in the laboratory with the exception of hydrazine hydrate which was purchased from Sigma-Aldrich Chemicals.

3.2 Preparation of the precursor solution

The precursor solution for the spray pyrolysis is prepared stepwise before arriving at the final solution. The steps are as below:

- A 0.02 M $CdCl_2$ solution is prepared by dissolving 4.8 g of $CdCl_2$ in deionized water and then diluting to one liter.
- Ammonia solution is prepared by dissolving ammonium hydroxide from the concentrated solution in deionized water in a ratio of 1:4.
- A 0.02 M solution of tellurium dioxide is made by dissolving 3.2 g of tellurium dioxide in ammonium hydroxide and diluting it to one liter (this process is slow and requires at least 6 hours for the telluride dioxide to dissolve completely).
- To about 100 ml of telluride dioxide solution in ammonium hydroxide, 1.0 ml of hydrazine hydrate is added.

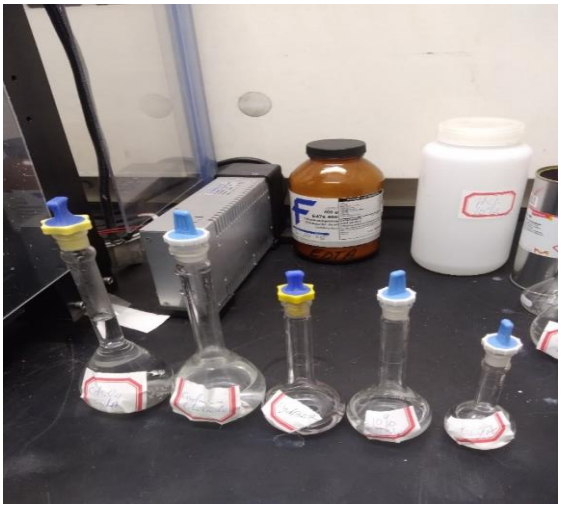

Figure 14: The spray solutions before mixing.

- A 0.2 M solution of EDTA was prepared by dissolving 5.845 g of EDTA in 80 ml distilled water and topping up with distilled water to 100 ml.
- 50 ml of the cadmium chloride solution is poured into a beaker.
- In the same beaker, 50 ml of telluride dioxide solution (with hydrazine) was added to the beaker. This resulted in a milky mixture.

- 1.0 ml of EDTA is added to this solution, then followed by adding both the ammonia solution and 0.1 M HCl alternately to adjust the pH to 11.5.
- This now gave a clear solution that was used as the precursor spray solution.
- 1.0 ml of platinic chloride was added to 50 ml of the resulting solution when it was required to produce platinized CdTe films.

3.3 Substrate preparation

In this work, stainless-steel SS 304 substrates are used. The steel substrates were first cut into 3 cm by 4 cm sizes using the tinsnips metal cutter. The cut pieces were first washed with a detergent; then they were thoroughly rinsed with deionized water. The steel plates were then placed in 10% v/v HCl solution for about two minutes to remove any residual oxide layer and rinsed again with deionized water. They were then dried in the oven at a temperature of 70 ^{o}C.

3.4 Spraying and sprayer settings

An INVENT3D spraying machine built to accommodate an air brush sprayer was used in this experiment. The unit has a horizontal bed where the substrate is placed. This bed has a heating circuit so that its temperature can be raised to about 250 ^{o}C. There is also a specially designed heater for the heater plate where the substrate is placed. This plate can be heated to a temperature of over 500 ^{o}C. The heater plate can be lowered or raised to vary the distance between the air the brush and the substrate. The air brush is fixed directly above the substrate heater plate. The unit also contains of a control dial located at the base next to the LCD screen where all settings can be adjusted. The LCD screen shows the settings made and monitors the progress of an assigned job. The printer also has a container for holding the spray solution and a protective cover on all sides.

An electric pump pressurizes and sends the carrier gas (air) over the precursor solution reservoir which is used to draw the solution into the spray nozzle.

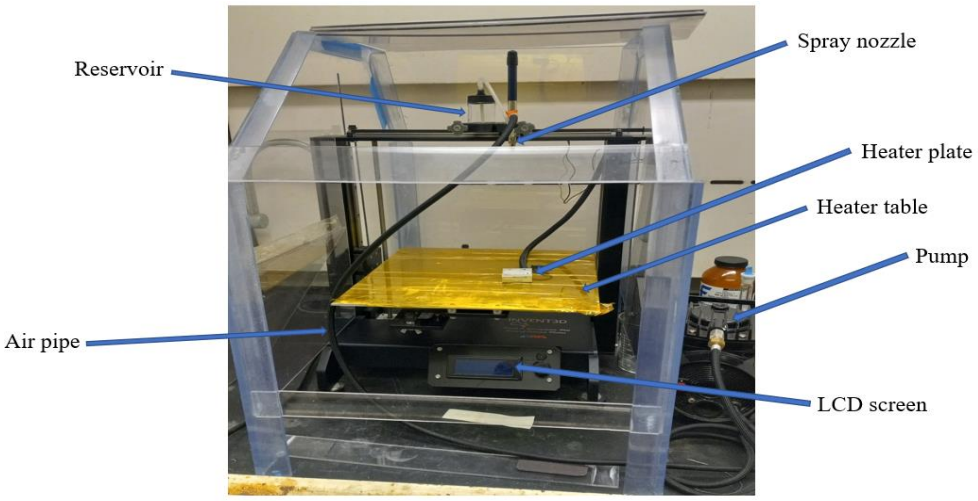

Figure 15: Images of the printer and the pump

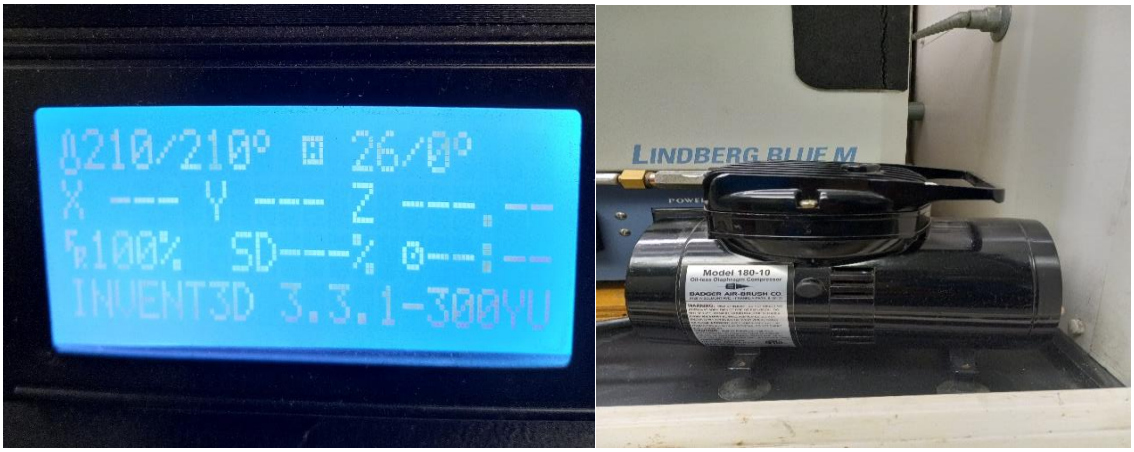

Figure 16: close-up images of the LCD screen and the air pump

3.5 The spraying process

This was the most crucial stage of the fabrication of the CdTe films. Different parameters were carefully set to ensure uniform films were produced. The most important parameters that were controlled to control the quality of the films were:

- Temperature of the substrate
- Annealing temperature
- The time of spraying
- Concentrations of the solution components
- Use of $CaSO_4$ instead of $CdCl_2$
- Platinizing the CdTe films.

The precursor solution was placed in the holding container of the printer. The X, Y, and Z settings were set with the Z distance of 25 cm from the nozzle to the substrate.

The cleaned steel substrate was placed on the heater plate and the temperature of the heater plate was set to 300 ^{0}C. When this temperature is achieved, the pump was switched on to spray the substrate for 3 minutes, maintaining a flow rate of 3.0 ml/min. Once the spray was complete, the pump was switched off and the substrate was allowed to cool. This process was carried out strictly in the fume hood with the correct personal protective equipment on since cadmium vapors are toxic. The films produced by the spray pyrolysis had the characteristic black color of cadmium telluride.

The CdTe-coated substrate is then annealed in an oven for 30 minutes at a temperature of 350 ^{o}C. According to Alonzo-Medina et al., annealing the sample causes relaxation and intrinsic stress liberation and reorganization with temperature.[46]

The procedure of spray pyrolysis was repeated for many other stainless-steel 304 substrates at different conditions listed above. This produced films of varying textures, surface morphology, color, and stability against peeling off. To investigate the properties of the produced films, several characterization procedures were performed.

3.6 Characterization of the CdTe film

3.6.1 XRD studies

This is a technique that is used for the identification of crystalline materials. It is a technique based on constructive interference of X-rays at the crystalline sample lattice. The X-rays are produced in the X-ray tube where a stream of electrons is produced at the cathode through thermionic emission. The electrons are converted to X-rays after colliding with a metal target. The X-rays produced are filtered to produce monochromatic X-rays and directed to the sample. X-rays are chosen because their wavelength is similar to the spacing atoms in a sample. The X-rays are diffracted as they bounce off the atoms in the structure making them change direction through an angle θ. Constructive interference of the X-rays creates X-rays of larger amplitude leading to a greater signal at that angle. The interaction of the X-rays with the sample produces constructive interference when Bragg's law is satisfied.[47]

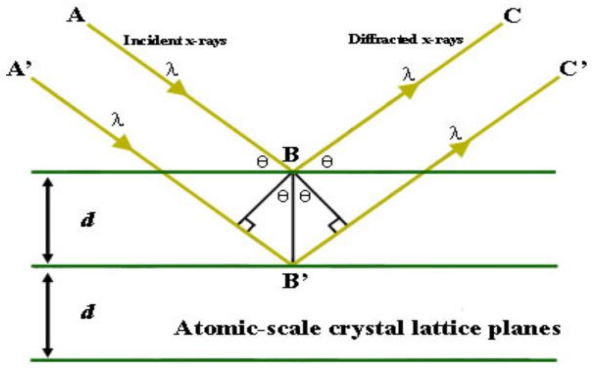

Figure17: X-ray diffraction showing incident X-rays, reflected X-rays, the diffraction angle θ, and lattice spacing d.[47]

Constructive interference of the diffracted X-rays happens when the distance between paths **ABC** and **A' B' C'** differ by an integer number of wavelengths (**λ**).

Below is Bragg's equation:

$n\lambda = 2\ d \sin\theta$, also $d = n\lambda/2 \sin\theta$

Debye's equation below can be used to calculate the average crystalline size.

$D = \frac{0.9\,\lambda}{\beta\ Cos\,\theta}$ where λ is wavelength of the x-rays

β is fullwidth at half maximum of the diffraction peaks

θ is Bragg's angle

The plot of the signal intensity against the various angles at 2θ positions is developed where the intensity of the signal signifies the abundance of the molecules in that specific phase. A thin peak usually corresponds to bigger and perfect crystal formations while a broader peak corresponds to a lack of perfect crystallinity. The sample is scanned through 2θ angles by which the possible diffraction directions of the lattice are attained. The conversion of the diffraction peaks to d-spacing makes it possible to identify the composition of the material.[47]

In this project, a Brucker XRD machine that uses copper target material for X-ray production is used. It is an instrument that is compact and easy to use with most of the operation remotely controlled from a computer.

The sample for testing is mounted on an aluminum disk. Before mounting the sample, the disk is first cleaned by wiping and then washed with methanol and dried. Some light petroleum jelly is smeared on the upper surface of the disk then the sample is firmly pressed on the jelly and leveled using a microscope glass slide. The disk with the sample is then transferred into the XRD chamber. The position of each specific sample is noted as there are six slots to run six samples in a row.

The parameters for running the sample are changed from the computer where the job is also executed. The time for running the sample may be adjusted; however, the least time is usually four hours per sample. Once completed, software called PWLD is used to convert the raw XRD data to a different format that is run on another software called EVA.DIFRAC. This final software gives an output that shows the signals at different 2θ angles. The intensity of the peaks, the lattice structure, the crystal phases, and the extent of crystallization can be obtained. A database in the software is then used to match the various signals of different crystal substances. In this project, the peaks of interest were those that may be cadmium telluride and the substrate. However, a spray pyrolysis at high temperatures may give rise to some other few peaks.

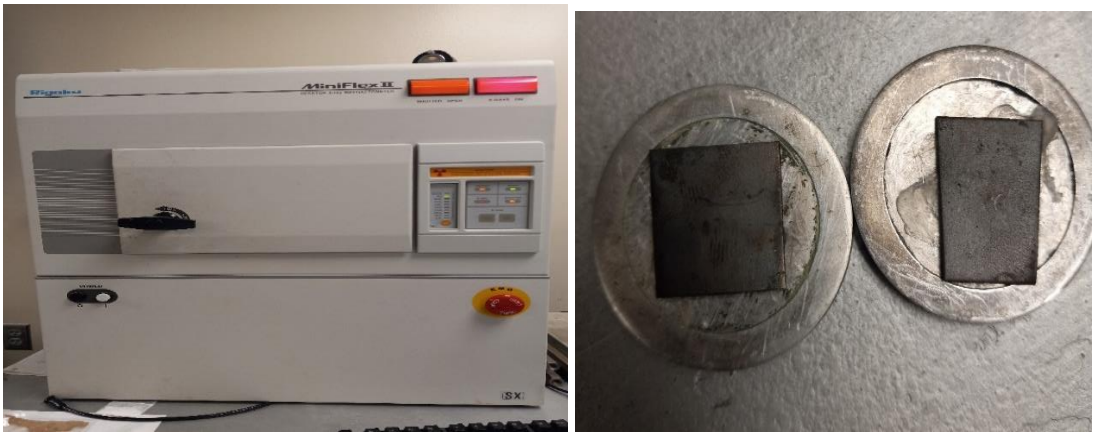

Figure 18: On the left; The Rigaku Miniflex II XRD machine. Right; the CdTe samples on the holders.

3.6.2 Scanning electron microscope (SEM)-EDS

SEM uses a beam of electrons instead of light to form an image in a process called raster scanning. The main parts of the SEM are:

The electron gun- this is the part that produces the electrons by thermionic emission from the cathode. The ejected electrons are accelerated and focused toward the sample by a set of anodes.

The condensers- a set of these adjusts the intensity of the electrons that finally reach the sample.

The objective lenses- focus the beam of electrons onto the surface of the sample.

Scanning coils- deflects the incoming electrons on the surface of the sample.

Detectors- The SEM uses several detectors to differentiate between -X-rays, secondary electrons, and scattered electrons. The detectors also play a great role in creating a magnified image.

The visual output system- this is the CPU and a monitor from which most of the commands are input into the SEM and also serve as the visual output. The elemental composition, crystal arrangement, percentage composition, and lattice phases among other types of data can be read and printed from here.

When the electrons impact the sample, they are slowed down and scattered.

Backscattered electrons (BSE)- these are electrons that come from deep below the surface of the sample which is some microns below the surface. These electrons strongly interact with the sample.

Secondary electrons- these come within a few nanometers from the surface of the sample and have less energy compared to BSE. These electrons are sensitive to the surface structure and provide the necessary topographic information.

This interaction of electrons and the sample reveals a lot about a solid sample including the surface morphology, the chemical(elemental) composition, the crystalline structure, and the orientation of the materials.[48]

In this project, SEM-EDS has been used to check the morphology of the film surface, used to perform a check on surface adherence and any presence of cracks or pinholes, used to check the

chemical composition of the thin film deposited, the percentage of each element in the film and the crystalline composition.

Figure 19: Scanning Electron Microscope, manufacturer JOEL JIB-4500 model.

3.6.3 Photoelectrochemical measurements: Cyclic voltammetry (CV) measurements

Cyclic voltammetry is an electrochemical measurement tool that provides a survey of the redox reactions. A cyclic voltammetry system consists of mainly the electrolytic cell, the potentiostat, and the display and control computer.

The electrolytic cell is a container in which the redox reactions takes place. It contains the working electrode (WE), the reference electrode (RE), the counter electrode (CE), and the electrolytic solution. The potential on the WE is varied but remains constant on the RE. The CE works in conducting electric current from the signal source to the WE. The electrolyte solution serves to provide ions and effect the charge transfer between the electrodes.

The electrolytic cell is connected to a potentiostat. The potentiostat linearly sweeps the potential between the WE and the RE. The measurements include varying voltage on the WE which is cycled between the two assigned potential limits. The set limits are supposed to cover both the oxidation and the reduction of the electroactive substance. When the sweep reaches the limit on one side, it sweeps at the same rate in the opposite direction. The scan rate is the rate of change of voltage with time and is given by volts/second (V/S). This process of sweeping the voltage with varying currents results in a plot called a voltammogram.[49]

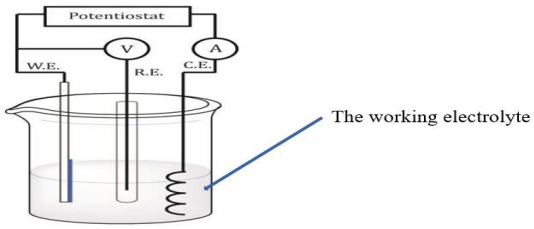

Figure 20: A schematic diagram of an electrolytic cell showing the working electrode (WE), reference electrode (RE), counter electrode (CE), potentiostat, and the working electrolyte.

In this research project, the working electrode in the electrolytic cell was the cadmium telluride thin film deposited on stainless steel 304 substrates. Cyclic voltammetry measurements were taken both in darkness and also under illumination by a xenon lamp, which simulates the solar spectrum to establish the photoactivity of the fabricated cell. The experiment was carried out in an acid medium in which the working electrolyte used was 1 M sulfuric acid (H_2SO_4). The counter electrode used was a platinum wire while the scan rate was maintained at 50 v/s.

(a) (b)

Figures 21: (a) The potentiostat and a laptop for operation, (b) The xenon lamp used to simulate sunlight.

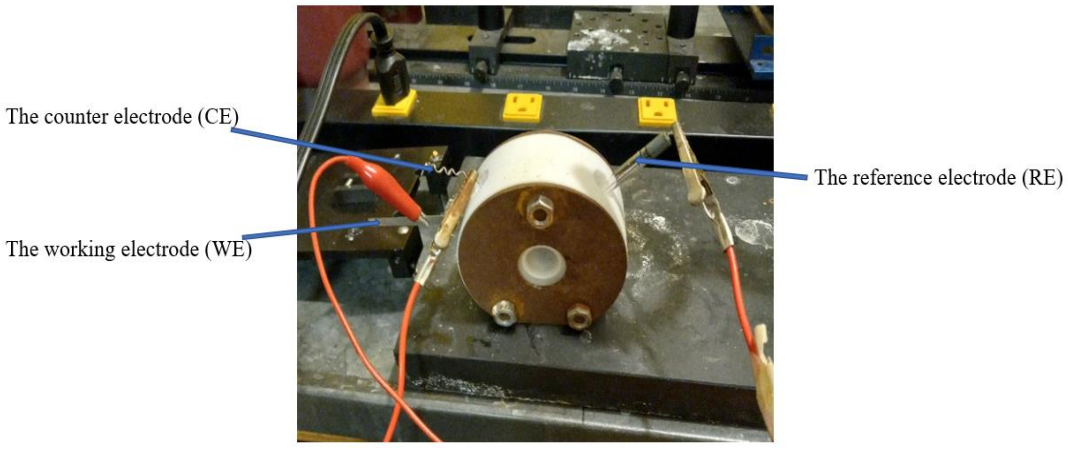

Figure 22: The electrolytic cell used for photoelectrochemical measurements

3.6.4 Profilometry analysis

Profilometry is used as a quantitative measure of surface roughness. The probe, which may either be mechanical or optical reads the contours on the surface of the sample. This gives the height of different regions from a certain common reference position. Through very delicate mechanisms of levers and a laser, each point is precisely marked and its height from the reference point is determined. This method can determine very small changes in the roughness of the surface to very few microns.[50]

In this project, profilometry was used to determine the thickness of the cadmium telluride film on the steel substrate. This project used the KLA Tencor-100 which is a very sensitive and comfortable device to work with. The sample was prepared by ensuring that one side of the sample plate had no film coating adhered to it. This created the reference point for any roughness of the film. The sample was placed on the sample stage plate. The control of the probe was done from the software on the computer. Most of the time the probe was set to scan 5 mm of the surface. The data generated was viewed and analyzed on the computer screen to attain the objective.

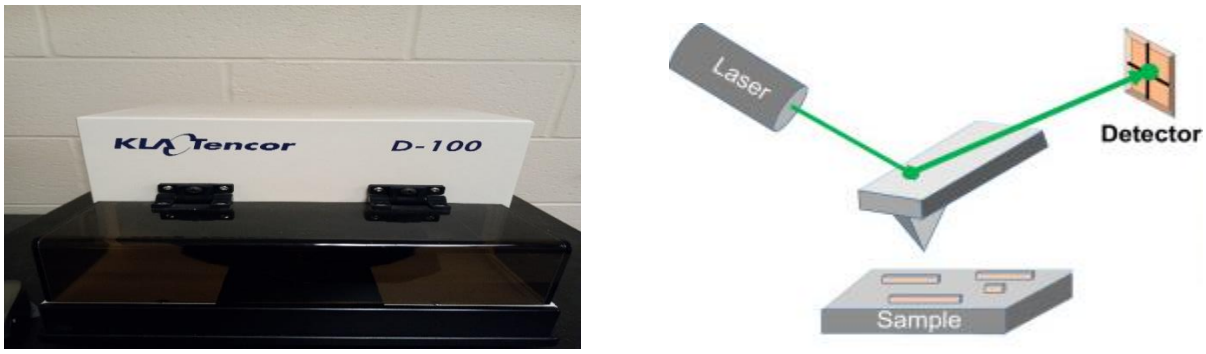

Figure 23: On the left, the KLA Tencor D-100 profilometer. Right, a basic schematic diagram of the profilometer.[49]

CHAPTER 4: RESULTS AND ANALYSIS

4.1 The spray pyrolysis process

A colorless solution for the spray pyrolytic deposition of CdTe on stainless steel 304 substrate was obtained by careful mixing of $CdCl_2$ and TeO_2 solutions at the same concentration and with EDTA added as a complexing agent. The complexing agent EDTA promotes reduced grain size and homogeneity, which the surface morphology depends on. This effect is due to the complexing agent increasing the total number of crystal nuclei produced in the deposition process so that smaller grains are generated. In addition, the complexing agent EDTA is less volatile and forms very stable complexes with metal cations which in this case means a stable complex with cadmium. This changes the process of growth of the CdTe to a slower one as the Cd^{2+} ions are slowly being released leading to a tellurium-rich surface. This leads to the production of the anticipated p-type semiconductor.

The spray produces droplets in the form of a mist in a process called nebulization. Each droplet undergoes pyrolytic decomposition which involves the breaking down of the droplet into its constituents. Because of the high temperature, all volatile materials, including the solvent, vaporize and leave behind the desired CdTe deposited on the surface. The surface temperature of the substrate is key to producing the desired films. The optimum temperature for the spray pyrolysis in this case is around 300 ^{o}C. This optimum temperature produces large closely packed grains as desired. Lower temperatures lead to the formation of non-uniform deposition and the substance is easily detachable. This results from the temperature being not sufficiently hot enough to decompose the sprayed droplets. On the other hand, very high temperatures >350 ^{o}C result in non-uniform deposition and results in pinhole defects. This is attributed to the high evaporation rate leading to the loss of some of the initial ingredients. This method produces

polycrystalline cadmium telluride, meaning that there are several types of crystals formed on the substrate surface.[42]

The spray process was carried out for 3 minutes at a constant rate of 3.0 ml/min. This is meant to ensure that enough material is deposited on the surface to prevent gaps in the CdTe film. The films deposited in this case showed a uniform surface coverage by observing with the naked eye, which provided some encouragement to confirm the result with other characterization methods. The distance between the nozzle and the hot substrate was kept at 25 cm.

4.2 Discussion on the spray pyrolysis reactions

Telluride dioxide dissolves in ammonia solution; this reaction is very slow and takes several hours for the tellurium dioxide to fully dissolve in the ammonia solution. In this experiment, all preparations involving this reaction were left stirring overnight with the spin bar to facilitate dissolving. Initially, the tellurium dioxide remains suspended but slowly the solution starts becoming clear as it dissolves. The dissolution of telluride dioxide in ammonia solution leads to the formation of tellurite ions (TeO_3^{2-}), in which tellurium has an oxidation state of +4.

$$2NH_4OH + TeO_2 \longrightarrow 2NH_4^+ + TeO_3^{2-} + H_2O \quad \text{..... (iv)}$$

Hydrazine was added to help in the reduction of Te^{4+} ions to Te^{2-} ions. Hydrazine in this experiment was used in its hydrated form where only 0.1 ml was used in 50 ml of tellurium dioxide solution.

$$2TeO_3^{2-} + 3N_2H_4 \longrightarrow 2\,Te^{2-} + 3N_2 + 6\,H_2O \quad \text{.....(v)}$$

The resulting solution was still colorless and was now ready for the next step.

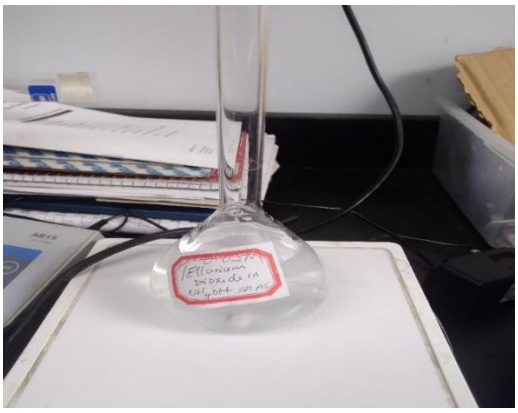

Figure 24: The colorless tellurium dioxide solution

Mixing the tellurium dioxide and cadmium chloride solutions produced a white precipitate which gives the mixture a milky appearance. The cadmium ions from $CdCl_2$ react with ammonia which was initially used as the solvent for telluride dioxide to form cadmium hydroxide which precipitates out. Initially, this solution had a pH of around 10. At this pH, the solubility of cadmium hydroxide is very low, hence a precipitate formed.

$$Cd^{2+}_{(aq)} + 2NH_3 + H_2O \longrightarrow Cd(OH)_{2\,(s)} + 2NH_4^{+}{}_{(aq)} \quad \text{.....(vi)}$$

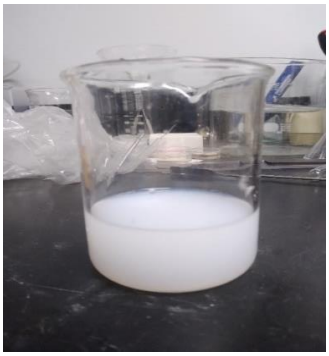

Figure 25: The white precipitate formed when $CdCl_2$ solution is mixed with TeO_2 solution in aqueous ammonia.

Ammonia solution is added dropwise till the solution turns colorless. Adding the excess ammonia solution introduces more ammonia which complexes with cadmium ions to form the complex, $[Cd(NH_3)_4]^{2+}$. The reaction equation is as shown in equation (iii) below.

$$Cd(OH)_2 + 4\,NH_3 \longrightarrow [Cd(NH_3)_4]^{2+} + 2\,OH^- \quad \text{.....(vii)}$$

The HCl solution helps to adjust the pH to the required pH of 11.5 which is the required pH of the precursor solution.

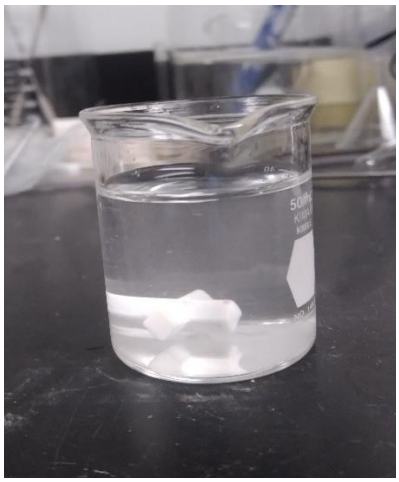

Figure 26: The colorless precursor solution

EDTA acts as the complexing agent and helps to promote clearly defined crystal growth. The presence of EDTA promotes reduced grain size and homogeneity. This effect is connected to the total number of nuclei generated during deposition. EDTA being less volatile and being able to react with the metal cation to form very stable complexes leads to the slow growth of CdTe due to the slow release of cadmium ions. This leads tellurium rich surface.

The pKas for the four carboxyl hydrogens in EDTA are 2.0, 2.7, 6.2, and 10.3. At pH 11.5, EDTA is fully deprotonated and mostly in the form $[EDTA]^{4-}$. A Cd^{2+} ion complexes with the deprotonated EDTA molecule to form a complex ion as shown in equation (viii) below.

$Cd^{2+} + [EDTA]^{4-} \longrightarrow Cd[EDTA]^{2-}$ ……(viii)

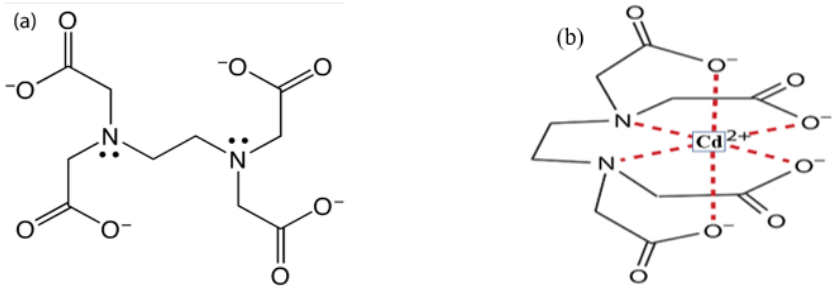

Figure 27: (a) Fully deprotonated EDTA; $[EDTA]^{4-}$ (b) Cadmium (II) EDTA complex

However, not all the Cd^{2+} ions are complexed with the EDTA. The number of moles of the Cd^{2+} that complex with EDTA can be worked out from the expression below:

Mol EDTA = M_{EDTA} x V_{EDTA} = M_{Cd} x V_{Cd} = mol Cd^{2+} where M is concentration, and V is the volume of the solution.

The concentration of EDTA used = 0.2 M, the volume of EDTA used = 1ml, the concentration of Cd^{2+} used = 0.02 M, and the volume of Cd^{2+} solution used = 50 ml. Thus, the moles of Cd^{2+}complexed can be obtained from the calculation below:

Moles of Cd^{2+} = moles of EDTA used = 0.2 x 0.0001

= 0.0002

Initial Cd^{2+} moles present = 0.02 x 0.005

= 0.001

The number of moles of Cd^{2+} not complexed with EDTA is 0.001-0.0002 = 0.0008 moles. The ratio of the complexed Cd^{2+} ions to the ones not complexed in this case is 1: 4. This means that

for every 5 Te^{2+} ions present, only four Cd^{2+} will be immediately available upon spraying as one is complexed and is slowly released. This leads to a tellurium-rich film. The moles of EDTA used can be varied depending on the requirements. However, it should be noted that the use of too much EDTA can lead to the deposition of too much elemental tellurium negatively affecting the crystallinity of the CdTe.

The telluride ions Te^{2-} react with the Cd^{2+} ions upon spraying to form a stable compound cadmium telluride which is deposited on the steel.

$$Cd^{2+} + Te^{2-} \longrightarrow CdTe \quad \text{.....(ix)}$$

The release of Cd^{2+} ions from the cadmium (II) EDTA complex can be represented by equation (ix) below:

$$[Cd(EDTA]^{2+} + Te^{2-} + 2OH^{-} \longrightarrow CdTe + [EDTA] + H_2O \quad \text{.....(x)}$$

All the volatile materials vaporize leaving behind the required CdTe adhered to the steel plate.

4.3 The fabricated films

The stainless-steel plates had a shiny metallic appearance before spraying. Upon spraying the precursor solution on the hot stainless-steel 304 substrate, some fumes were observed to be rising from the substrate. These were the volatile products at that temperature which mainly include water vapor, hydrogen chloride gas, and ammonia gases. These formed dense fumes further from the substrate indicating the presence of ammonium chloride on the cooler upper parts of the hood.[42]

The color of the substrate was progressively becoming darker in appearance with an ashy coating. This was due to the deposition of loosely adhered cadmium telluride. After allowing the

films to cool, it was noted that the films could easily be scraped off the surface of the substrate as if they were poorly attached.

Annealing of the films was done in the oven at a temperature of 400 ^{o}C for one hour. After the annealing, the films appeared to have a very dark crystalline surface, which was tightly adhered to the surface. According to Alonzo-Medina et al., annealing the sample causes relaxation and intrinsic stress liberation and reorganization with temperature.[46] This is what was actually noted in this experiment. The figures below (28-31) show a plain stainless-steel 304 substrate and the CdTe films on stainless-steel substrates deposited at different conditions.

(a) (b)

Figures 28 : (a) Plain stainless-steel 304 (b) As-deposited CdTe film (before annealing) (Deposited at 300 ^{o}C)

(a) (b) (c) (d) (e)

Figure 29: Annealed CdTe films (annealed at 350 ^{o}C). Deposited at (a) 300 ^{o}C, (b) 330 ^{o}C, (c) 350 ^{o}C, (d) Deposited at 250 ^{o}C, (e) Deposited at 200 ^{o}C



(a) Deposited at 300 ºC for 5 mins. (b) Deposited at 300 ºC for 5 mins. (c) Deposited at 350 ºC for 5 minutes.

Figure 30: CdTe films deposited at various temperatures for 5 minutes and all annealed at 350 ºC for 30 minutes.

Figure 31: Film deposited at 300 ºC using $CdSO_4$ instead of $CdCl_2$ and annealed at 350 ºC for 30 minutes

4.4 XRD results and analysis

4.4.1 XRD results for films fabricated at different temperatures.

XRD analysis was carried out to determine the crystal lattice phases, identify different peaks from the sample and determine the compounds in the sample represented by the different peaks. The main concern here was to pull out the peaks for cadmium telluride and their crystal phases. The library reference 2θ peak positions for cubic phase cadmium telluride are 23.7 (111), 39.3 (220), 46.4 (311), 57.0 (440), 63.0 (331) and 71.5 (422). This was matched by doing an XRD analysis of pure commercial cadmium telluride powder (Figure 32), which showed similar patterns. Most of the XRD patterns of the fabricated CdTe films showed peaks corresponding to the reference values and the values for pure commercial CdTe powder which indicates that the fabricated films had well-formed crystalline CdTe. However, the film composition was determined by the different parameters of deposition as discussed later in the chapter.

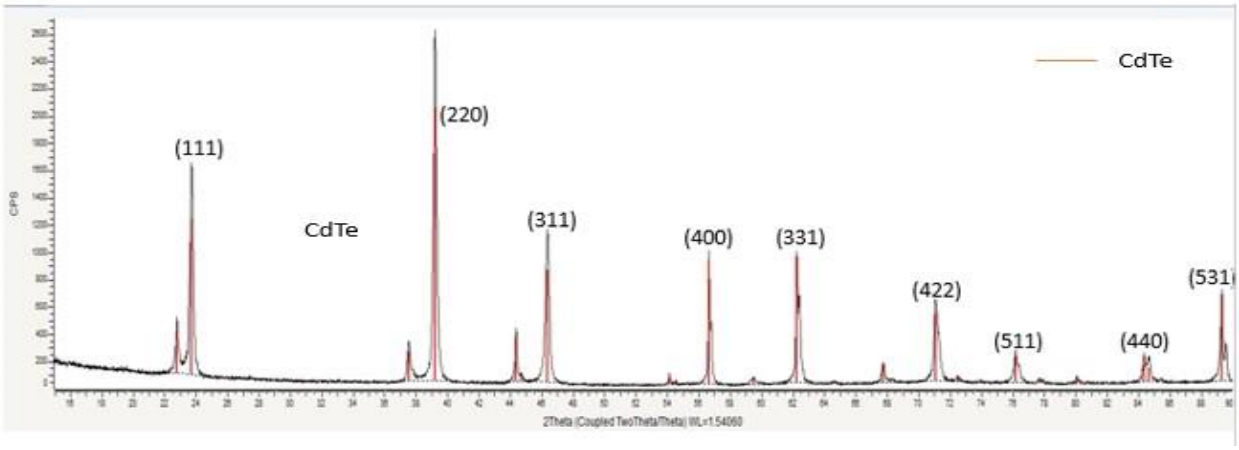

Figure 32: XRD peaks for the pure commercial CdTe from Sigma-Aldrich Chemicals.

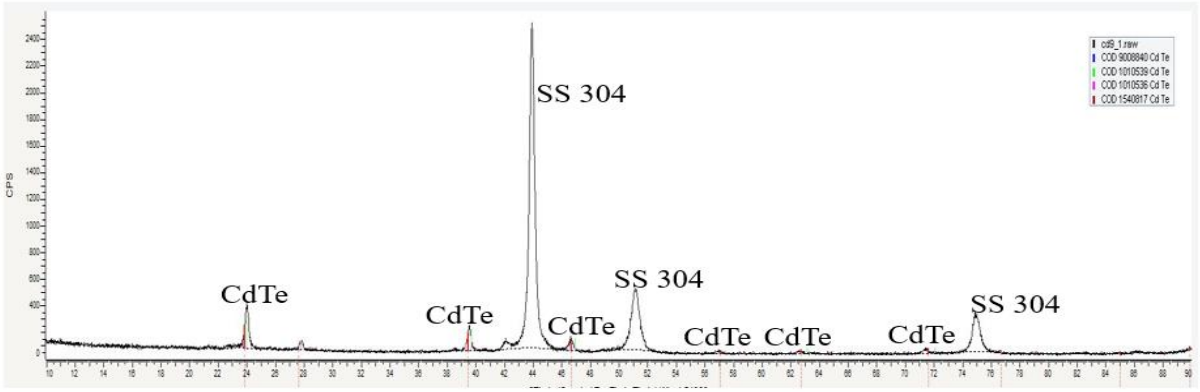

Figure 33: XRD pattern for CdTe (deposited at 300 ºC) and annealed at 350 ºC for 30 minutes

The pattern for fabricated CdTe thin film in Figure 33 above shows some significant peaks corresponding to the theoretical values and those obtained from running an XRD on the pure commercial CdTe powder. The peaks on the left were taller (higher intensity) and decreasing in height moving to higher 2θ values. The peaks appeared at positions 24.018, 39.583, 57.802 and 71.293 degrees. These values corresponded to 111, 220, 311, 400 and 422 lattice planes.

The other major peaks noted in this sample were mainly belonging to the stainless steel 304 substrate as compared to XRD patterns of the plain substrate and that of the theoretical values for stainless steel 304. From reference values, the stainless steel XRD gives three main peaks at 44.0, 50.5, and 75.0 values. The peaks correspond to 111, 200, and 220 *hkl* values (planes of the cubic phase). The intensity of the peaks also decreases from left to right indicating the domination of the 111-reflection plane.

From Figure 34 below, it can be seen that the stainless-steel substrate had 3 main peaks which correspond to the above values.

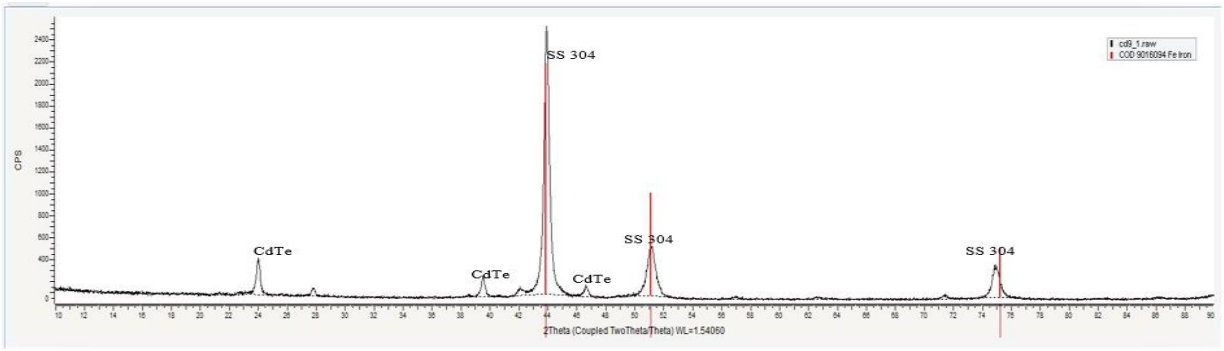

Figure 34: XRD analysis of the fabricated CdTe film showing the stainless steel 304 peaks only. Fabricated at 300 ºC and annealed at 350 ºC for 30 minutes.

From the above XRD patterns, it appears that the substrate peaks are dominating in intensity compared to the CdTe film on it. This is an indication that the deposited film is very thin and most of the X-rays pass through to the steel substrate, hence high-intensity values of the substrate material. It may also be an indication of lower crystallinity of the CdTe with some of it remaining in an amorphous form that will not be detected by the XRD analysis procedures.

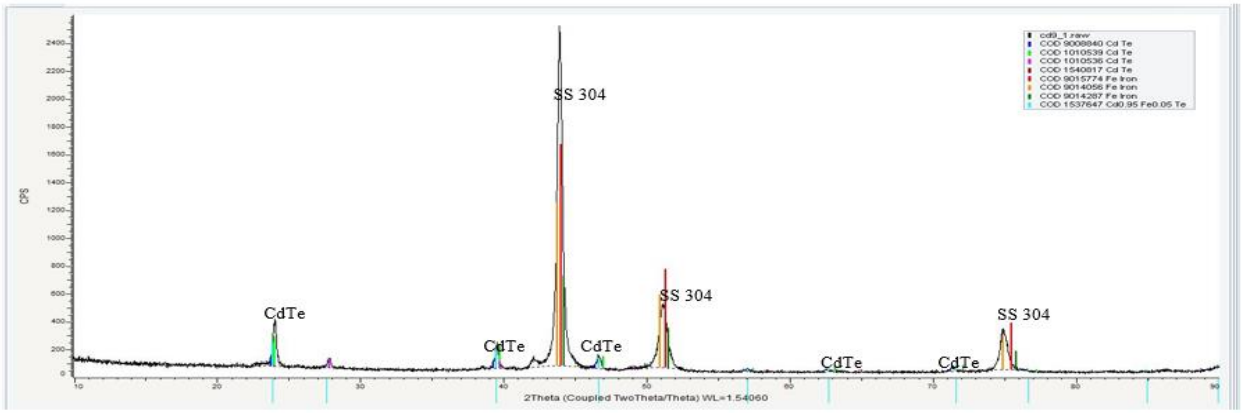

Figure 35: XRD analysis with all peaks labelled for the CdTe film deposited at 300 ºC and annealed at 350 ºC for 30 minutes.

From the XRD pattern shown in Figure 35 above, it is clear that all the peaks belong to either the substrate or the deposited CdTe. However, accompanying the CdTe peaks is a compound of the

formula $Cd_{0.95}Fe_{0.05}Te$. This is mainly CdTe with 5 Fe atoms to 95 Cd atoms substituted with Fe. This formation is significant in the performance of the film as it improves the electrical contact between the stainless steel and the film.

At 250 ºC and maintaining a mixture of equal volumes of 0.02 M $CdCl_2$ and 0.02 M TeO_2, the peaks obtained are as shown in Figure 36 below.

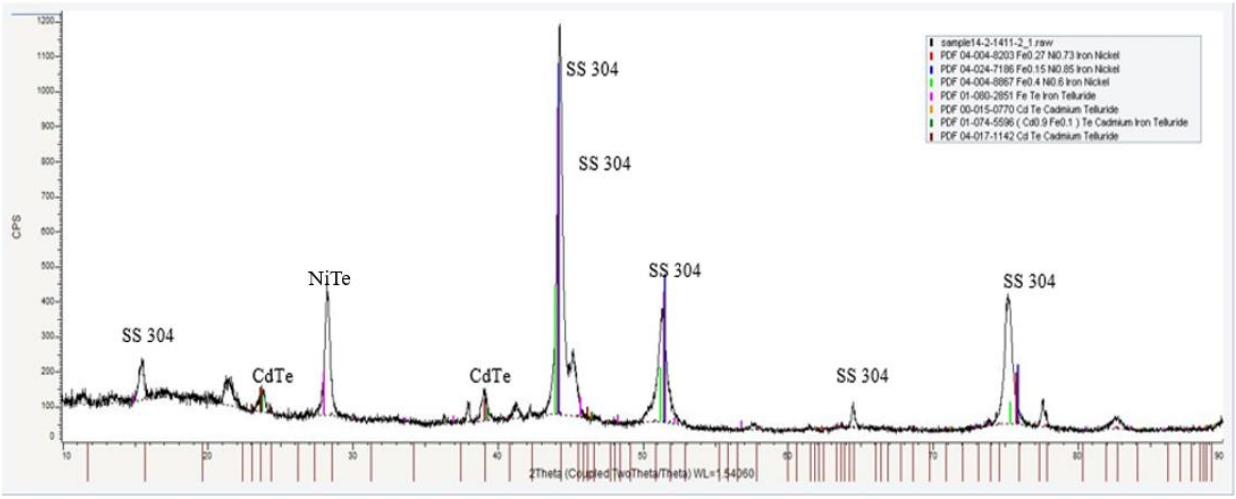

Figure 36: XRD analysis for the sample deposited at 250 ºC and annealed at 350 ºC for 30 min.

When a film was deposited at 250 ºC and annealed, the XRD analysis shows little crystalline cadmium telluride. This means that this temperature can also promote the generation of substantial crystalline CdTe. However, the peaks are small and the surface is noted to contain nickel telluride and some cadmium iron telluride as shown on the legends at the top right of Figure 36.

When the substrate temperature was kept at 200 ºC, the XRD image is as shown in Figure 37 below.

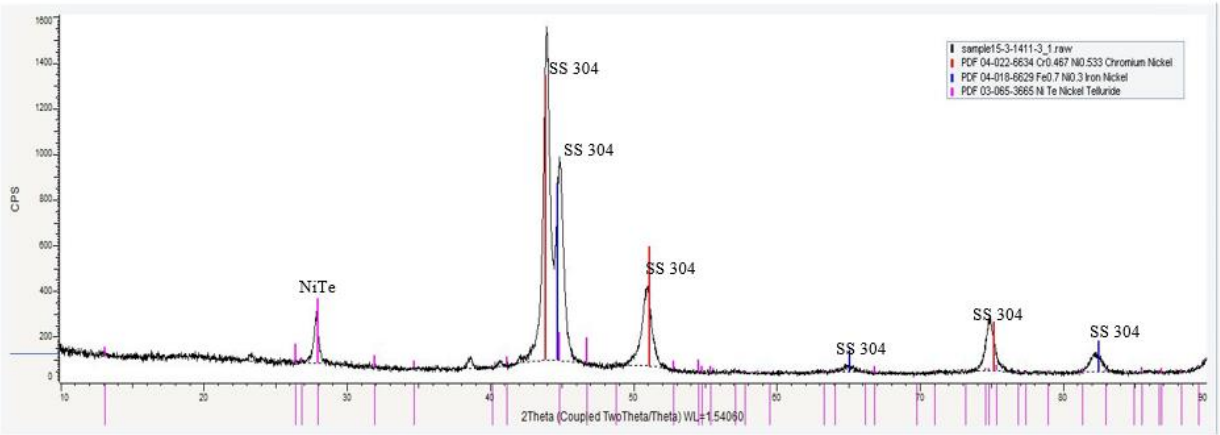

Figure 37: XRD analysis of the deposition at 200 ºC and annealed at 350 ºC for 30 minutes.

At 200 ºC, there was no peak of cadmium telluride produced. This reveals that at this temperature, the spray pyrolysis method cannot be used to deposit crystalline CdTe films on a stainless-steel substrate. At this low temperature, very few volatile substances will be formed and the process is more like just dampening the substrate surface with solution. However, it was noted that some nickel telluride formed.

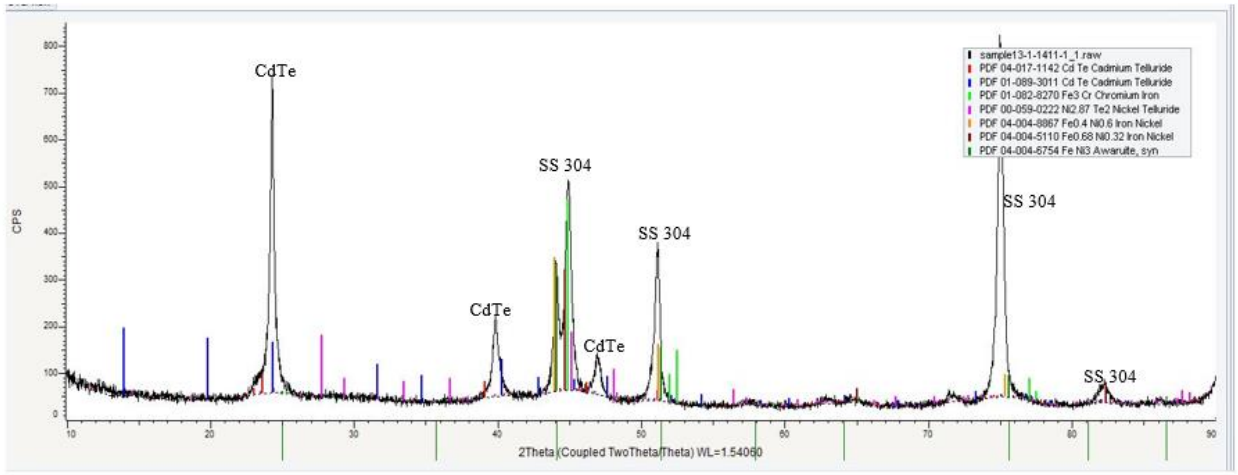

Figure 38: XRD analysis for sample deposited at 330 ºC annealed at 350 ºC for 30 minutes

CdTe peaks are noticeable at points 24.0, 40.0, 47.0, and 57.0 angles. The CdTe peaks are well-defined, have high intensity, and overshadow those of the stainless-steel substrate. This is an

indication of the presence of good CdTe crystallinity which is also an indication of good deposition conditions. The presence of the stainless-steel peaks also indicates that the film is still very thin on the surface. These stainless-steel peaks are seen at 44.0,45.0, 51.0, 75.0, and 72.0 degrees.

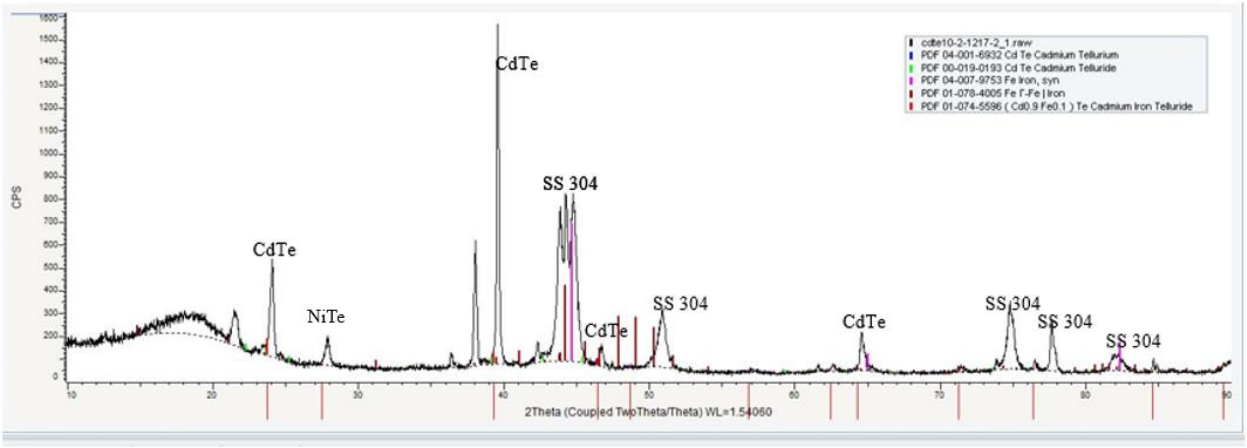

Figure 39: XRD analysis for the CdTe film fabricated at 350 ^{o}C and annealed at 350 ^{o}C for 30 minutes.

At 350 ^{o}C, sharp CdTe peaks were obtained at positions 24.0, and 39.5 degrees only. These correspond to the 111 and 220 lattice planes of the cubic phase.

4.4.2 Effect of change of concentration of the precursor solutions

When the concentration of the precursor solution was changed to lower values of 0.01 M and 0.015 M from the initial concentration of 0.02 M, and the spray time maintained at 3 minutes with the spray rate still at 3.5 ml/min the following data was obtained as shown in Figure 40 and Figure 41 below.

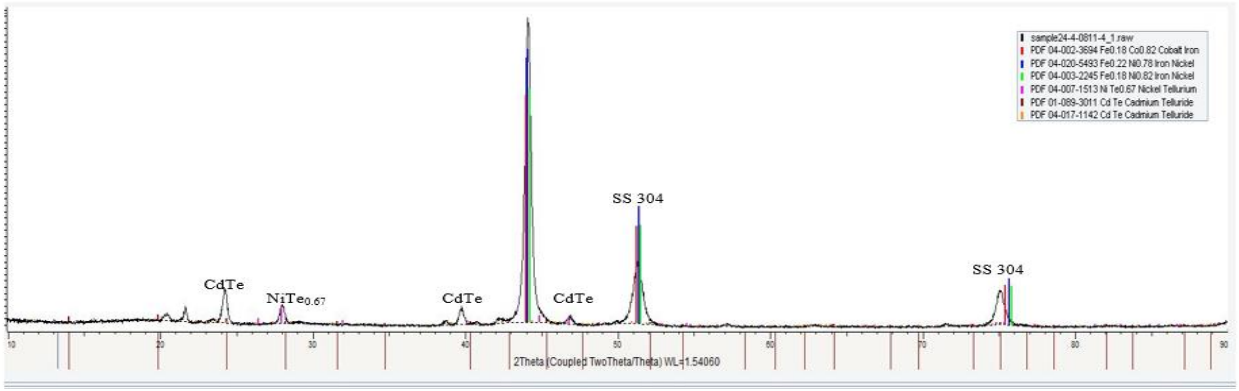

Figure 40: XRD analysis for dilute solutions at 0.01 M $CdCl_2$ and 0.01 M TeO_2 at 300 ^oC and annealed at 350 ^oC for 30 minutes.

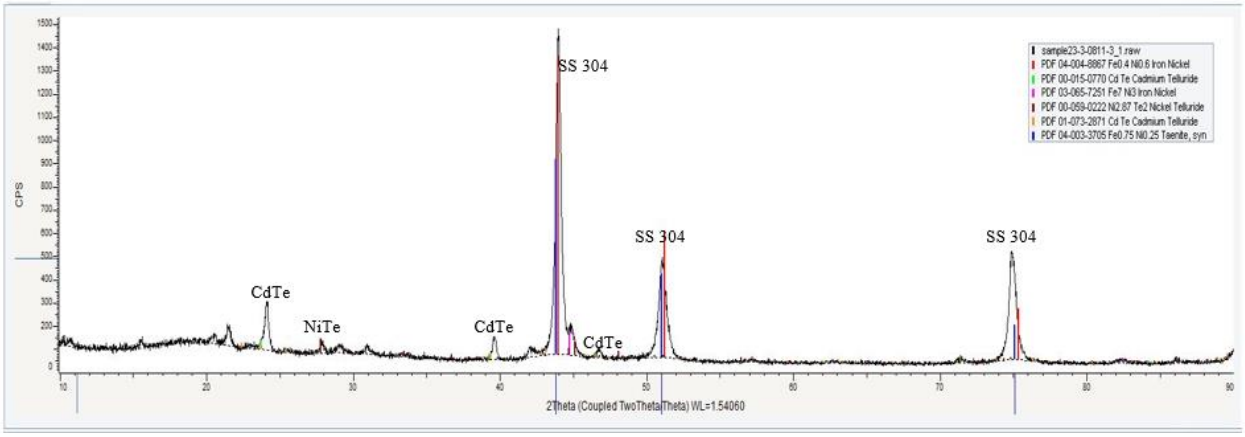

Figure 41: XRD analysis for dilute solutions at 0.015 M $CdCl_2$ and 0.015 M TeO_2 at 300 ^oC and annealed at 350 ^oC for 30 minutes.

The XRD analysis of the resulting film shows very weak peaks of CdTe implying the formation of a very thin film as less material is deposited over that same time. The weak signals could also be indicative of surface imperfections from widely dispersed materials with a high evaporation of most of the materials in the solution.

4.4.3 Effect of time of deposition

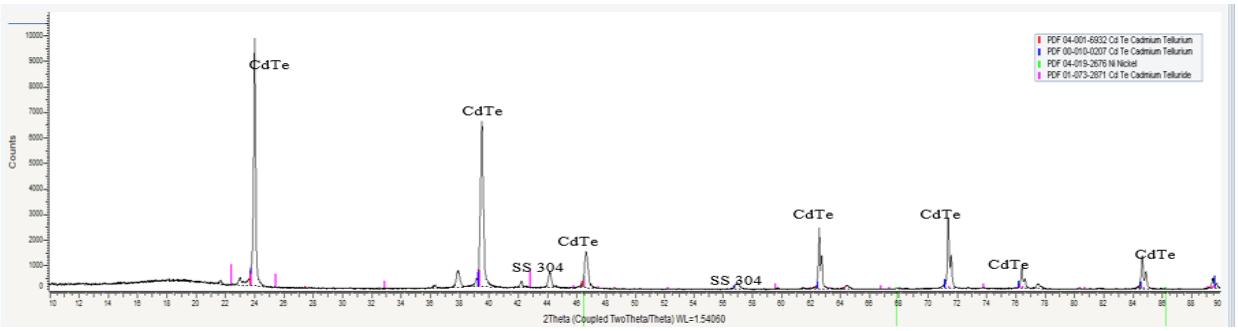

Figure 42: XRD analysis for the CdTe film deposited at 300 ^{o}C with a spray time of five minutes and annealed at 350 ^{o}C for 30 minutes.

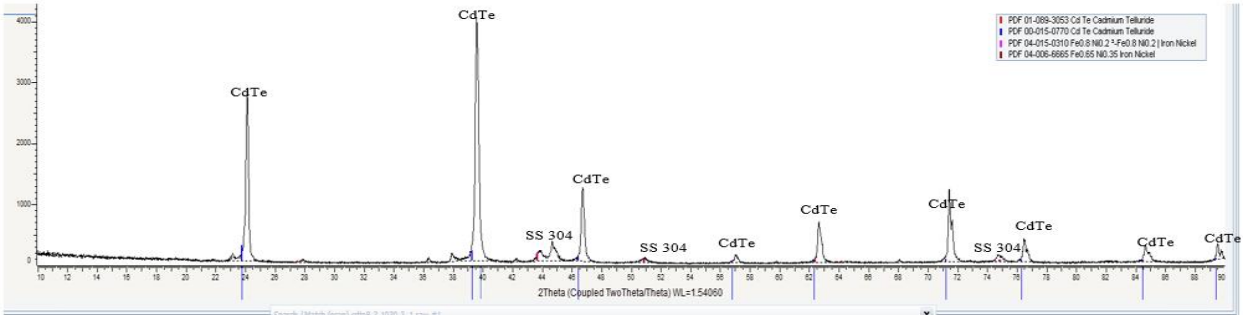

Figure 43: XRD analysis for the CdTe film deposited at 330 ^{o}C with a spray time of five minutes and annealed at 350 ^{o}C for 30 minutes.

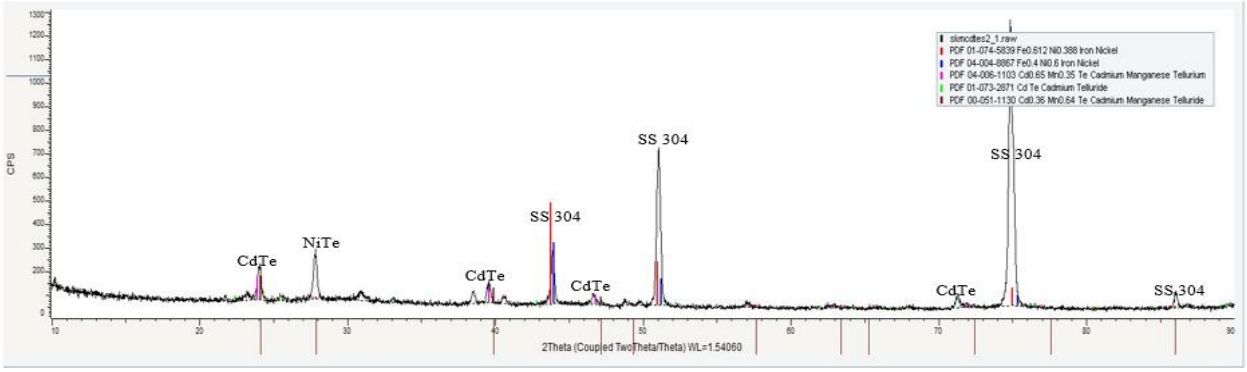

Figure 44: XRD analysis for the CdTe film deposited at 330 ^{o}C with a spray time of 2 minutes and annealed at 350 ^{o}C for 30 minutes.

From Figure 43 and Figure 44, it can be observed that the time of spraying affected the height of the CdTe signal. The CdTe peaks in these two figures are very strong and dominate over the stainless-steel peaks. This can be majorly attributed to the thickness of the film and more material being deposited over the extended time. This increases the depth the X-rays have to penetrate before interacting with the stainless-steel substrate. However, crystallinity is more important than thickness as more thickness is a waste of material because theoretically, only a few microns are required for photoactivity in CdTe films. It was clearly observed from the XRD patterns that the fabricated films were composed mainly of well-crystallized cadmium telluride. The data obtained from the films had all the cadmium telluride films matching with EVA.DIFRAC existing data for cubic phase CdTe. However, it was noted that the CdTe peaks obtained in all samples were slightly shifted to the right from the exact center of the database positions. This could be attributed to the orientation of the samples and sample placement in the XRD instrument.

From the different conditions of temperature and concentration used, there were some significant differences observed from each condition. The films fabricated at 300 ^{o}C and annealed at 350 ^{o}C for 30 minutes showed prominent strong peaks for the CdTe. The same was observed for the films fabricated at 330 ^{o}C. There was no substantial difference for films fabricated at 350 ^{o}C. For the sample deposited at 250 ^{o}C, the peaks observed were very small even after annealing. This implies very little crystalline CdTe is present. For the film deposited at 200 ^{o}C, there was no CdTe peak observed as shown above in Figure 37. This implies that no crystalline CdTe was formed and probably no CdTe was formed at all. This is due to the failure of full decomposition of the precursor solution and most of the materials that were expected to vaporize did not.

Therefore, from these observations, the ideal temperature for spray pyrolytic deposition of CdTe is steel in a range between 300 ºC and 350 ºC.

The stainless-steel peaks were observed in all the films where they majorly appeared at three positions of 2θ. Stainless steel was not part of the film fabricated, however, the films were very thin on average a few microns. This made it possible for the X-rays to penetrate the thin surface hence the stainless-steel signals. It may be expected that, with the high temperature of the spray, annealing the samples may not be necessary as the crystals may form instantly. However, from the XRD results, it has been proven that annealing the samples led to higher intensity of the CdTe signals implying more crystallinity than the unannealed films. The spray time was too short (between 2 minutes and 3 minutes) and could not allow good crystal formation hence annealing was necessary. Figure 45 below shows the XRD results for the platinized CdTe film.

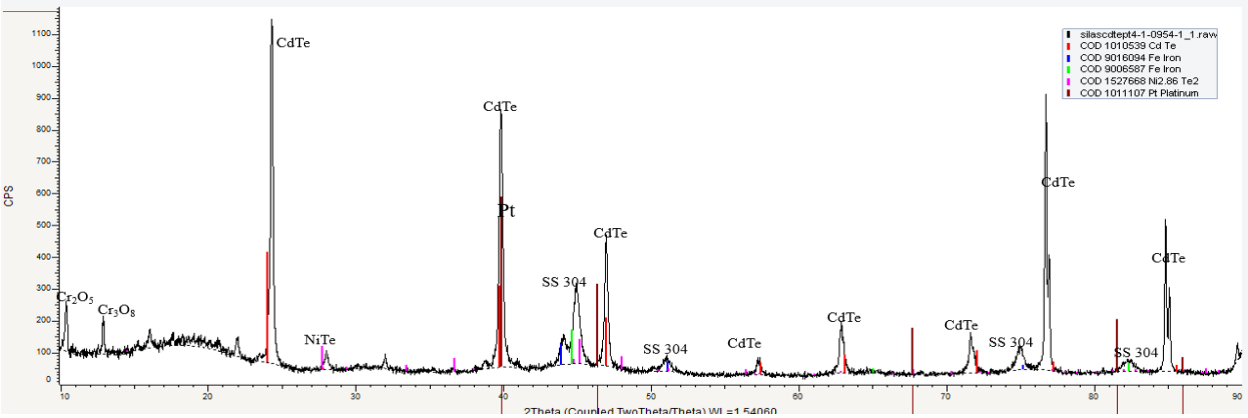

Figure 45: XRD analysis for the platinized CdTe deposited at 300 ºC and annealed at 350 ºC for 30 min.

From Figure 45 above, CdTe peaks were observed, and a platinum peak was obtained at 40 degrees corresponding to (111) *hkl* in the cubic phase. Peaks of Cr_2O_5 and Cr_3O_8 were also observed. This was due to the reduction of Pt^{2+} to Pt^0 and the oxidation of Cr to Cr^{3+}.

4.5 SEM analysis

The surface morphology of the fabricated CdTe films was studied through SEM. The images show well-formed particles and grain boundaries for most of the films. However, with very low deposition temperatures (200 ^{o}C), the crystals did not appear distinct in the boundaries, meaning there was less crystallinity. This is deduced from the EDS data that shows the presence of cadmium and tellurium but no good crystal boundaries were observed even with the annealing. This demonstrates the need for optimum temperatures in the initial deposition.

The films deposited at temperatures of 300 ^{o}C, 330 ^{o}C and, 350 ^{o}C showed good crystal formation and clear grain boundaries. This is an indication that the optimum temperature for the pyrolytic deposition of CdTe on stainless-steel 304 films is between 300 ^{o}C and 350 ^{o}C and not a fixed temperature.

The elemental composition was also noted from the SEM-EDS results. Cadmium and tellurium were found in varying quantities in different films. However, tellurium had a higher atomic percentage than cadmium. This means that the films were rich in tellurium and hence a p-type semiconductor had been fabricated.

In addition to the cadmium and tellurium, stainless-steel elements were also noted in all the films. Since the films deposited were very thin, some of the X-rays were ejected from the substrate beneath the film, hence they formed part of the elemental analysis output. The Stainless-steel elements that feature in the analysis were Fe, Ni, Mn, Cr, and C. In addition to these elements, extra carbon, oxygen, and chlorine were noted to be present. The extra carbon is a residual product from EDTA after the pyrolytic deposition and could also be from ambient air and its effect on the film quality may need to be studied independently. The oxygen present in the

films is due to surface oxidation since the spray pyrolysis was carried out in ambient air. The chlorine noted in the films is residual from $CdCl_2$ and the HCl used. The effect of these elements on the performance of the films need to be studied too.

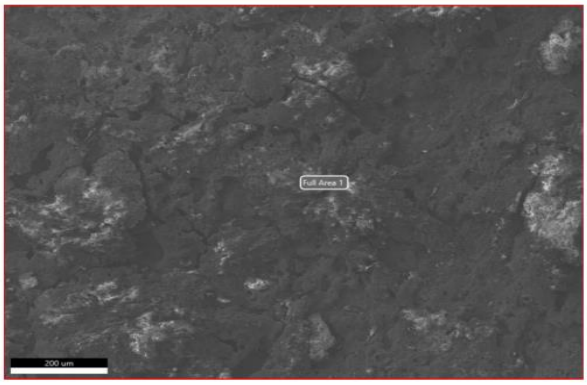

Figure 46: SEM image of CdTe film deposited before annealing (As-deposited)

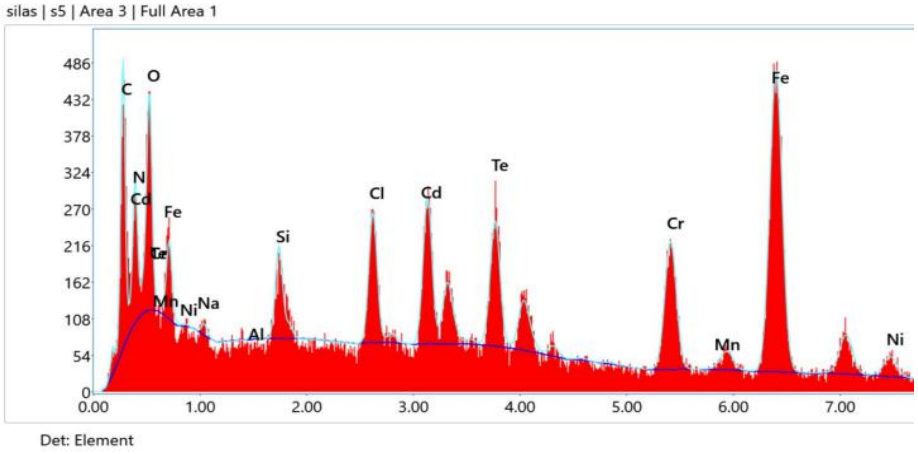

Element	Weight%	Atomic%
C K	17.12	51.16
N K	6.35	12.18
O K	6.51	10.32
Cl K	2.15	1.42
Si K	1.10	1.01
Cr K	2.27	1.35
Fe K	27.13	13.19
Cd L	13.21	3.81
Te L	15.19	4.16

Figure 47: EDS analysis for the as-deposited films deposited at 300 ^{o}C.

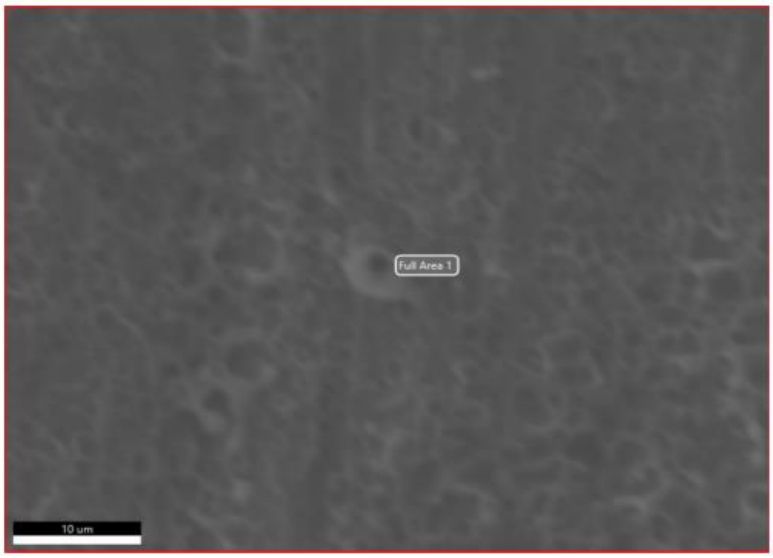

Figure 48: SEM analysis for CdTe film deposited by spray pyrolysis at 300 ^{o}C and annealed at 350 ^{o}C for 30 minutes (magnification x7500).

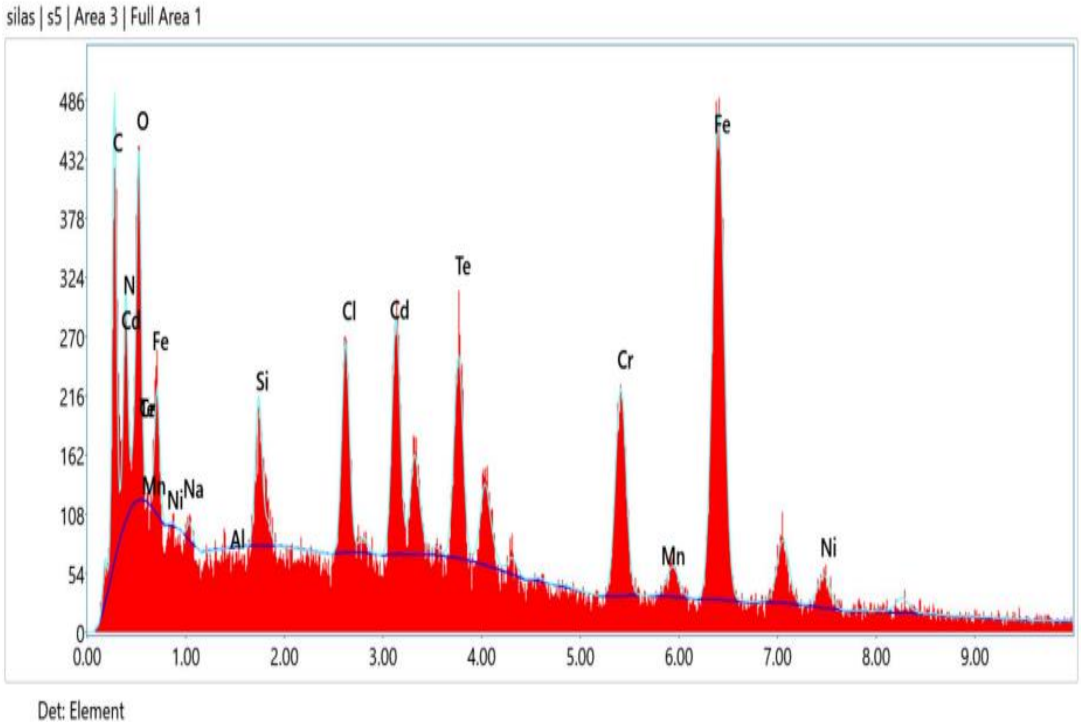

Element	Weight%	Atomic%
C K	23.43	50.21
O K	7.28	13.38
N K	6.56	10.56
Si K	0.28	10.01
Cl K	2.26	1.64
Cr K	7.61	3.76
Mn K	0.35	0.17
Fe K	29.37	13.54
Ni K	3.30	1.45
Cd L	8.08	1.85
Te L	10.33	2.08

Figure 49: SEM-EDS elemental analysis for CdTe films deposited at 300 ^{o}C and annealed at 350 ^{o}C for 30 minutes.

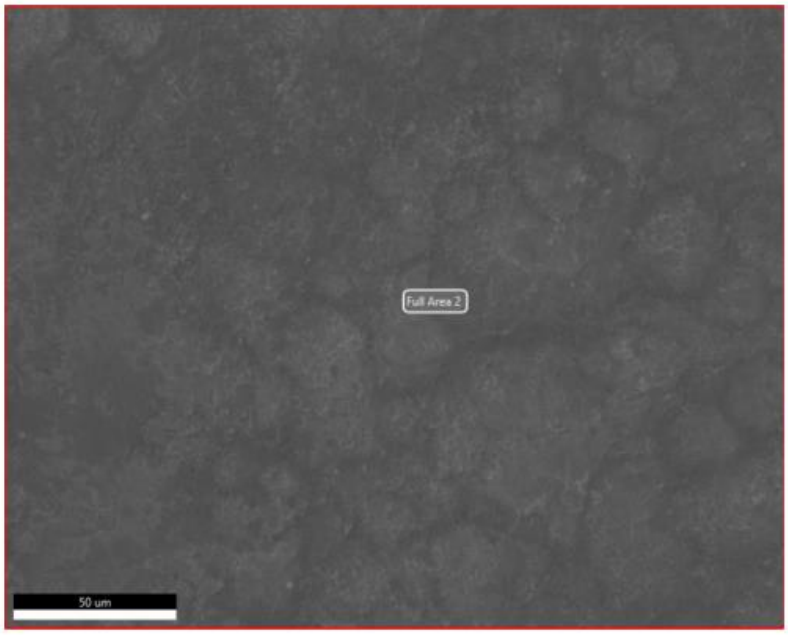

Figure 50: SEM analysis for CdTe film deposited at 330 ^{o}C and annealed at 350 ^{o}C for 30 minutes (magnification x2500)

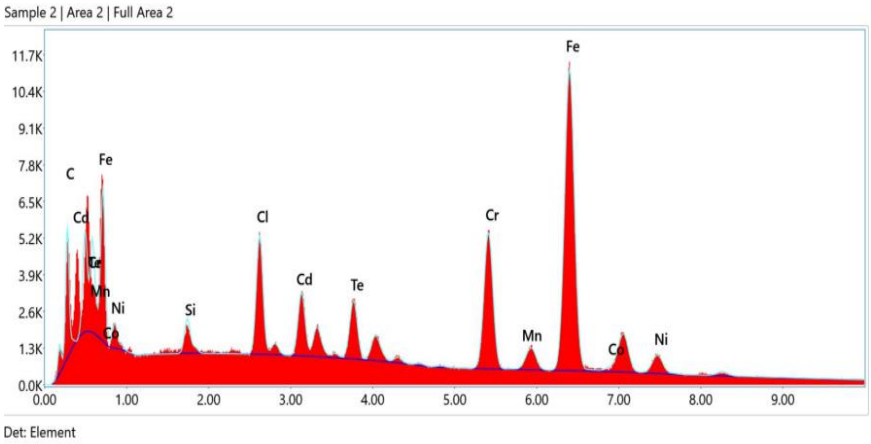

Element	Weight%	Atomic%
C K	20.77	56.09
Si K	0.67	0.77
Cl K	3.18	2.91
Cr K	11.81	7.36
Mn K	0.97	0.57
Fe K	44.65	25.93
Co K	0.85	0.47
Ni K	4.59	0.40
Cd L	5.33	1.54
Te L	7.18	1.82

Figure 51: EDS analysis for CdTe film deposited 330 ºC and annealed at 350 ºC for 30 minutes.

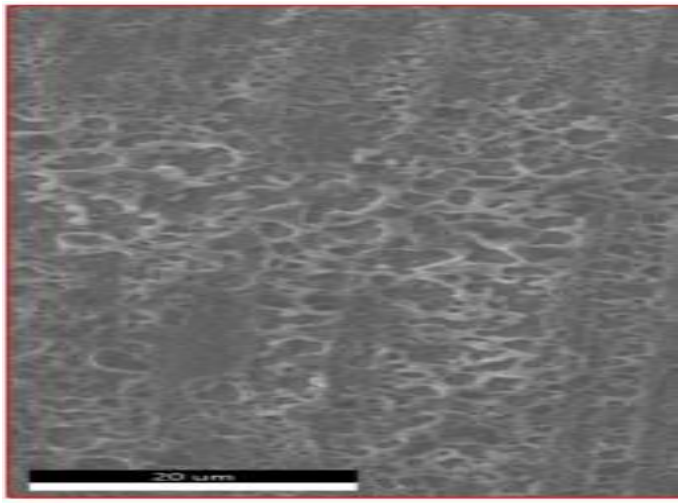

Figure 52: SEM analysis of CdTe film deposited at 350 ºC and annealed at 350 ºC for 30 min. (magnification x5000)

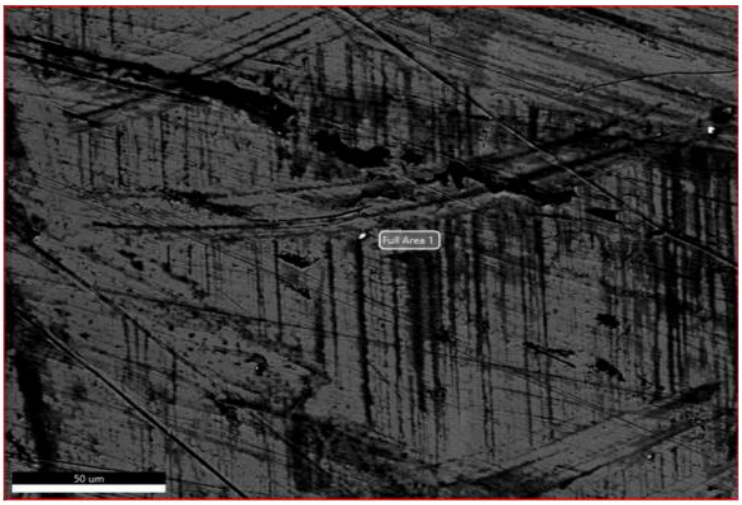

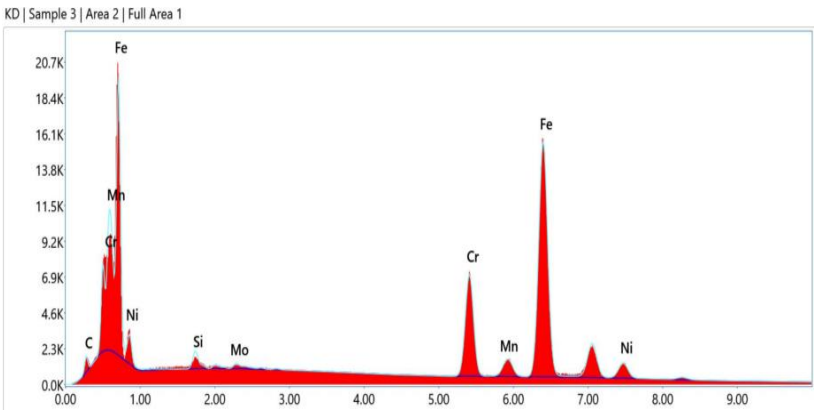

Element	Weight%	Atomic%
C K	5.6	21.65
Si K	0.71	1.16
Cr K	15.73	13.85
Mn K	1.84	1.53
Fe K	67.99	55.72
Ni K	7.42	1.82

Figure 53: SEM and EDS analysis of plain stainless-steel substrate (magnification x2500).

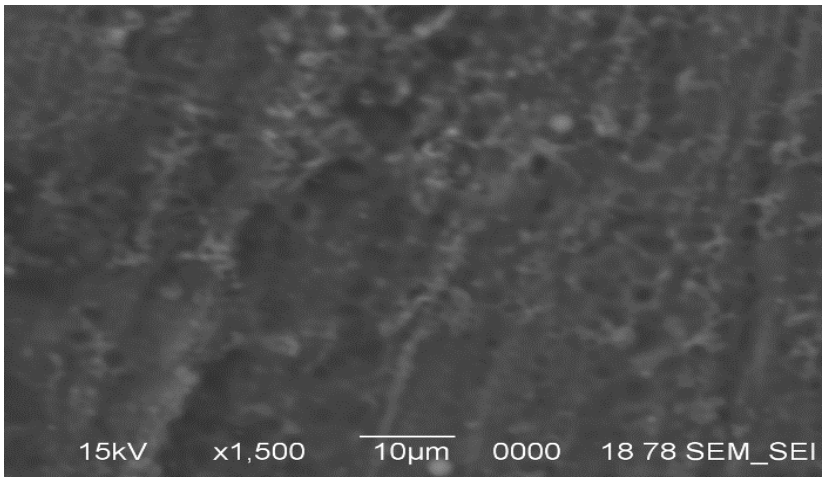

Element	Weight%	Atomic%
C K	21.13	62.48
N K	0.16	0.28
Si K	0.44	0.56
Cr K	8.03	4.38
Mn K	0.57	3.61
Fe K	27.11	25.45
Ni K	2.82	14.34
Cd L	16.65	4.00
Te L	22.85	4.35

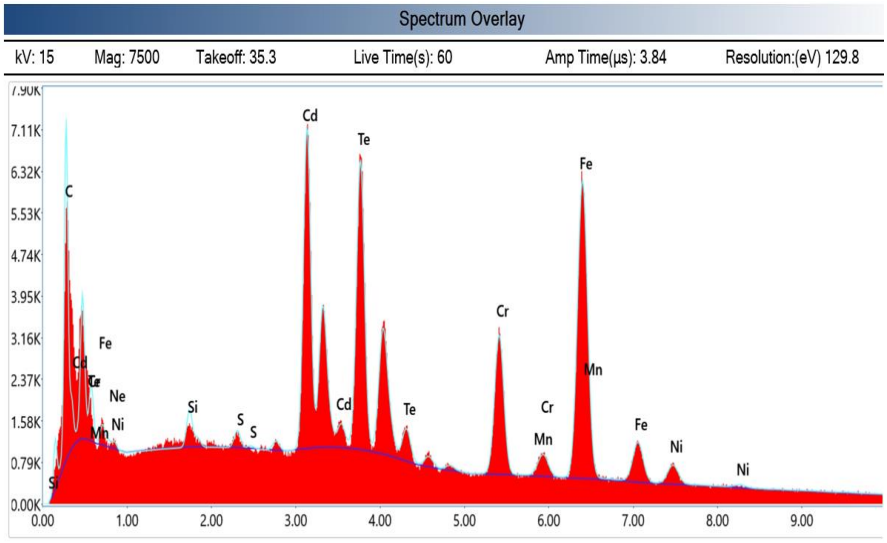

Figure 54: SEM-EDS analysis for CdTe films on stainless steel substrates deposited at 300 ºC for 5 minutes and then annealed at 350 ºC for 30 minutes.

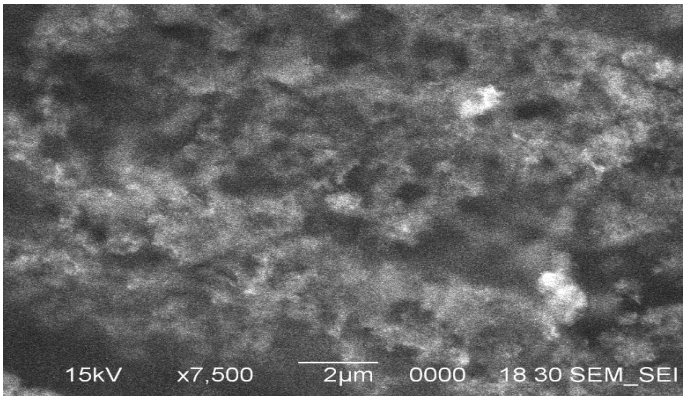

Figure 55: SEM analysis for CdTe films deposited at 200 ºC and annealed at 350 ºC for 30 minutes.

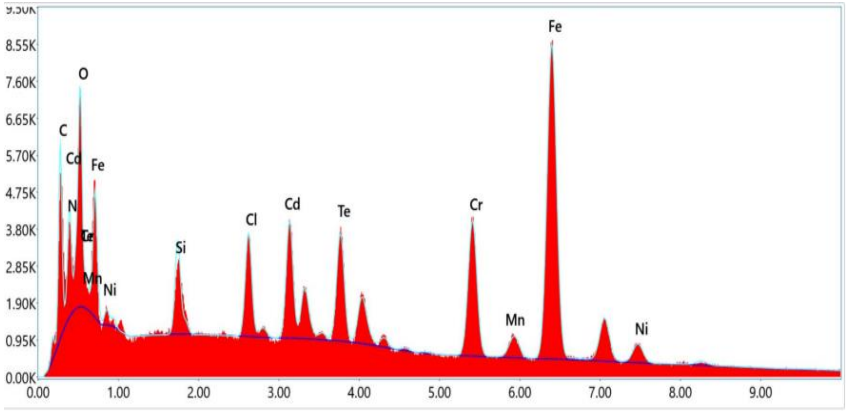

Element	Weight%	Atomic%
C K	19.72	45.01
N K	5.81	11.72
O K	6.71	11.86
Cl K	2.03	1.62
Cr K	8.93	4.85
Fe K	34.72	17.58
Ni K	3.45	1.66
Cd L	7.29	1.83
Te L	9.96	2.21

Figure 56: EDS analysis for the sample deposited on the stainless-steel substrate at 200 ºC and annealed at 350 ºC for 30 minutes.

4.6 Profilometry analysis results

Profilometry analysis was done on the deposited films to determine their thickness. It was noted from the results obtained that the spray pyrolysis method produces thin films on the order of a few microns. The films in this project had an average thickness of about 10 microns. From the profilometry analysis, it is seen that the spray pyrolysis method used in this project was successful at producing quite thin and uniform films with very small surface variations. Very thin films imply that very little material was used to deposit the films and that the film would have a shallow depth for light absorption. The figures below (57-63) show the profilometry results for the CdTe films deposited at various temperatures and annealed at 350 ^{o}C for 30 minutes.

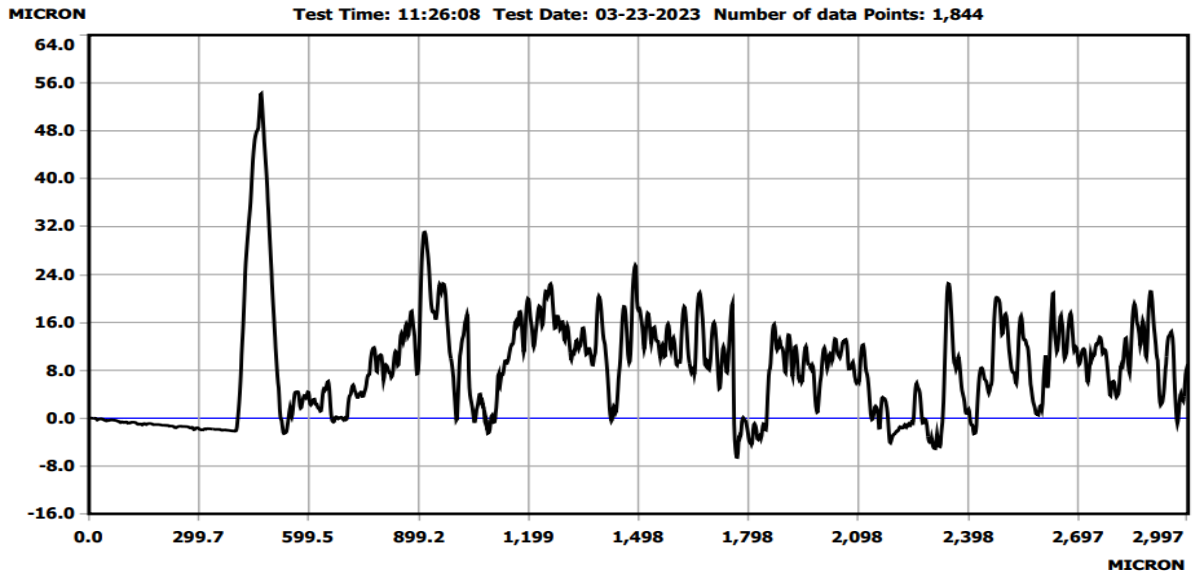

Figure 57: CdTe Sample sprayed at a substrate temperature of 250 ^{o}C for 3 minutes. The average film thickness of about 4 microns.

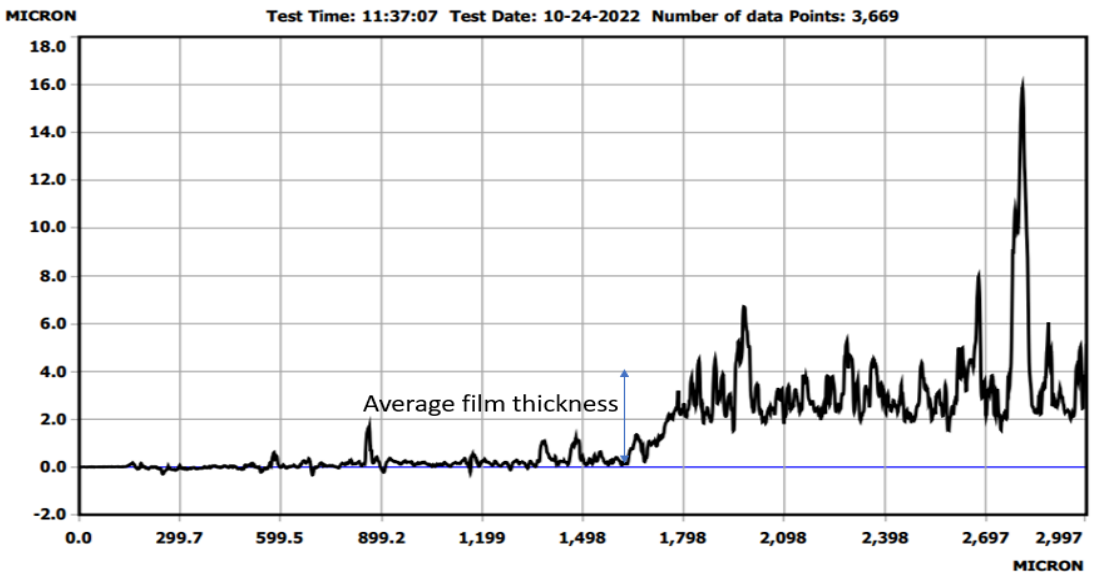

Figure 58: CdTe film deposited at 300 ºC for 3 minutes. The average film thickness of about 3 microns.

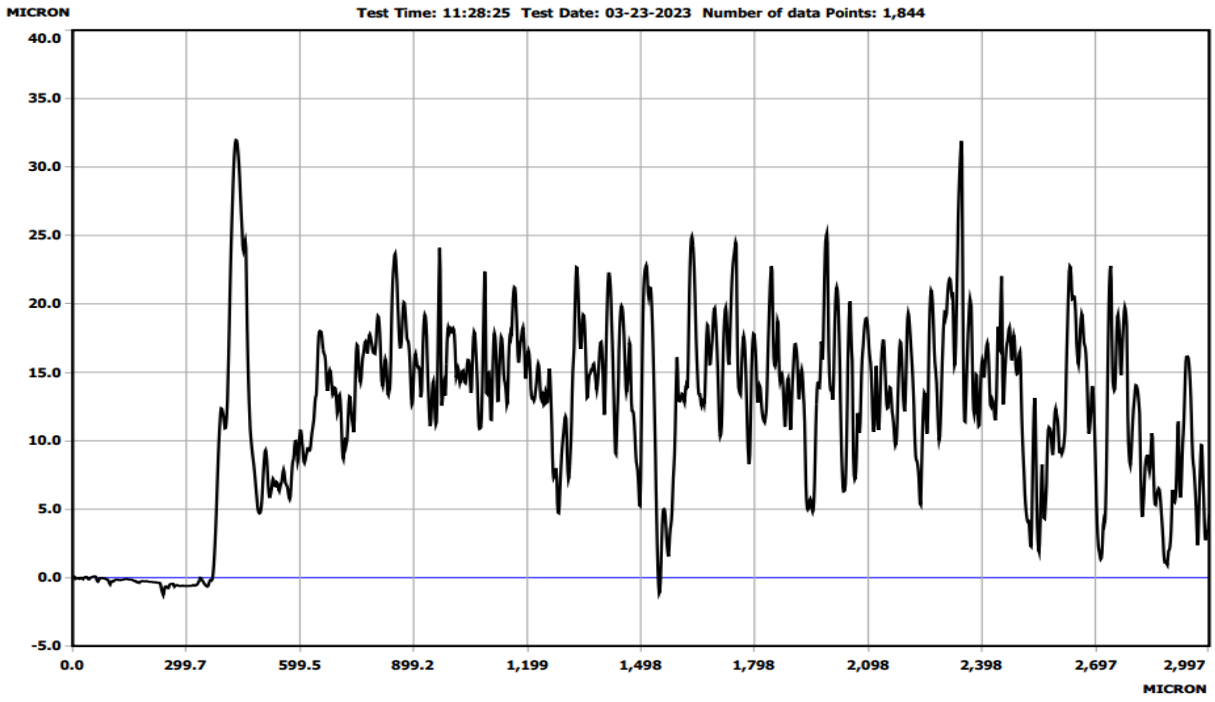

Figure 59: CdTe film deposited at 330 ºC for 3 minutes. The average film thickness of about 13 microns.

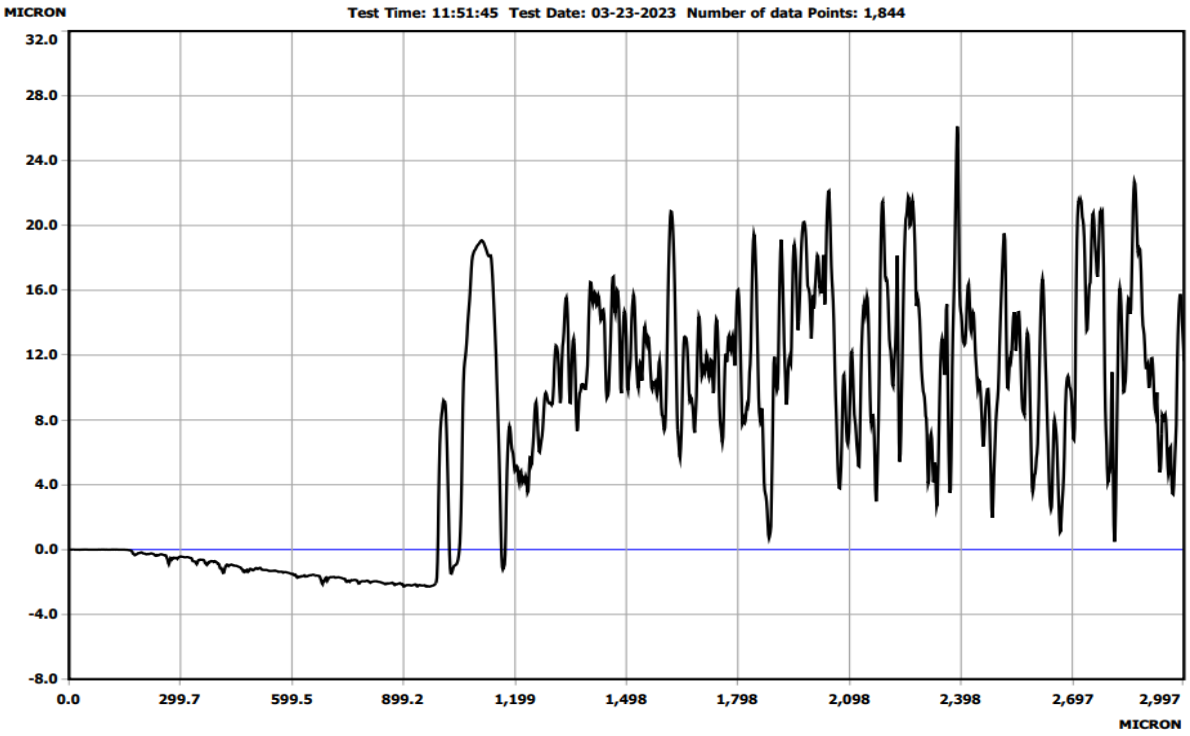

Figure 60: CdTe film deposited at 350 ºC for 3 minutes. Average film thickness of about 7 microns.

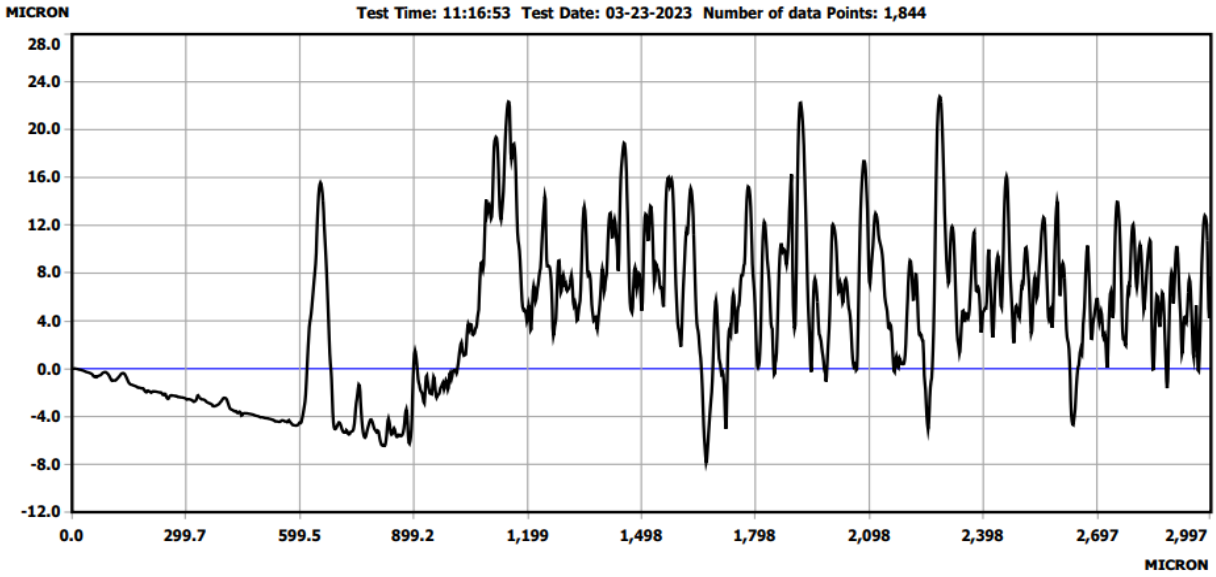

Figure 61: CdTe film deposited at 250 ºC for 5 minutes. Average film thickness of about 10 microns.

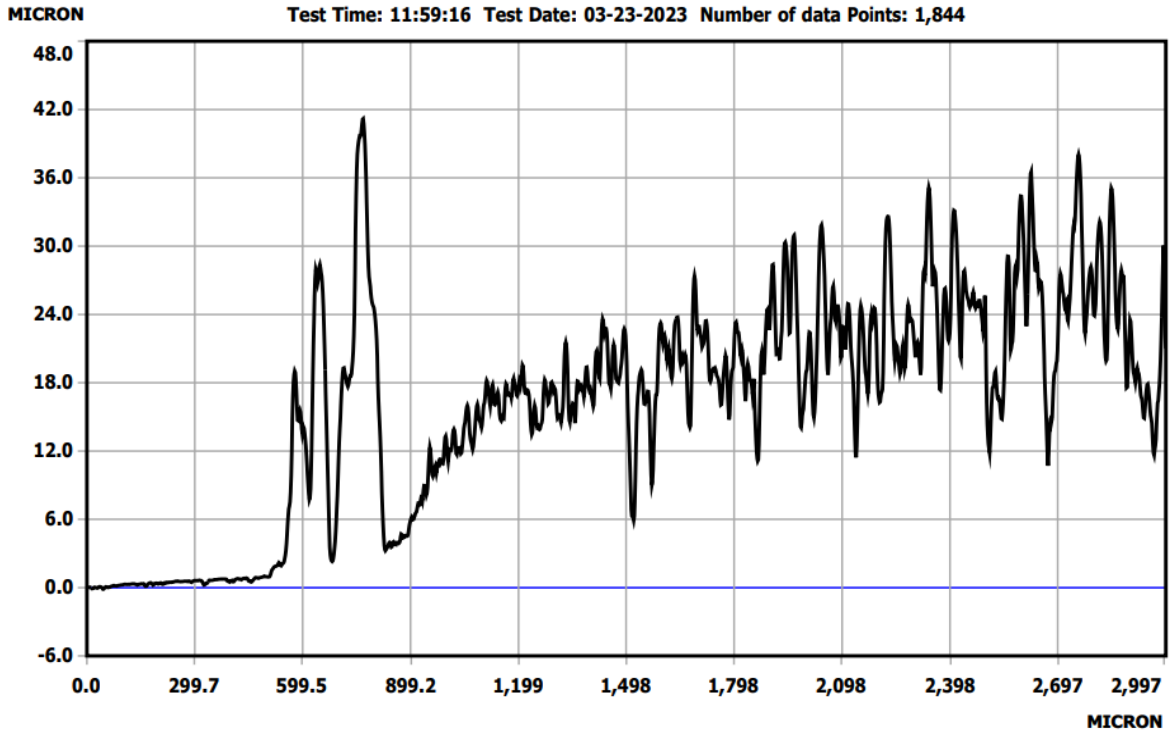

Figure 62: CdTe film deposited at 300 ºC for 5 minutes. The average film thickness of about 16 microns.

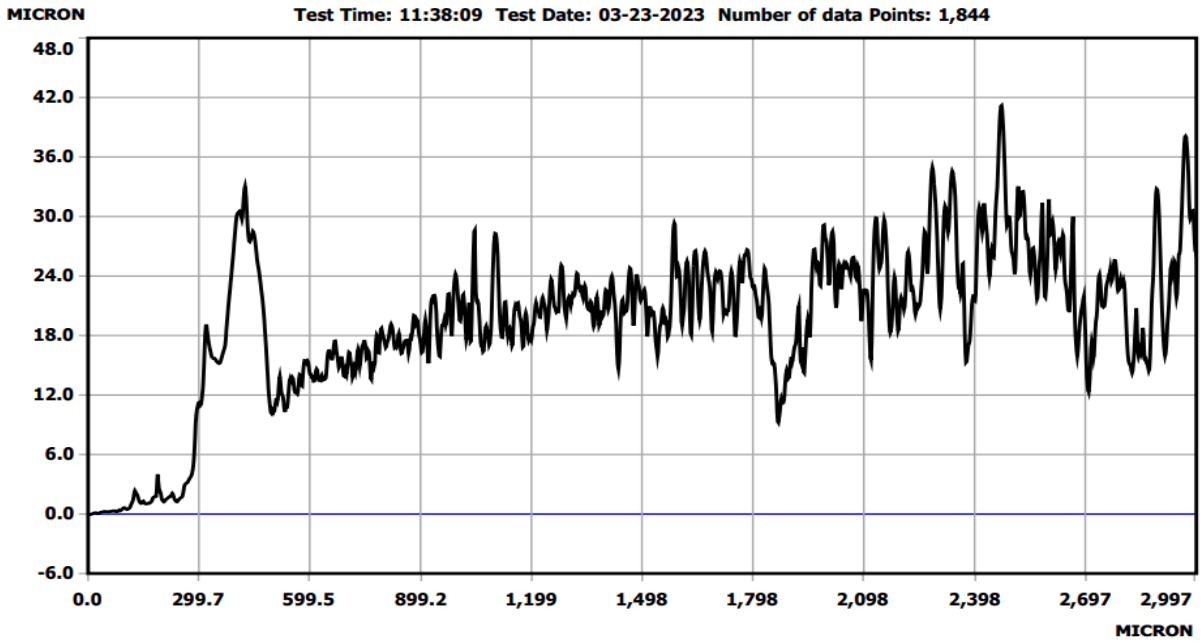

Figure 63: CdTe film deposited at 330 ºC for 5 minutes. The average thickness of about 18 microns.

4.7 Photoactivity analysis: cyclic voltammetry (CV) and linear sweep voltammetry (LSV)

CV was performed for the fabricated cadmium telluride films to determine their photoactivity. There was a notable redox reaction when both the steel and CdTe samples were used. In all the cases, platinum electrode was used as the counter electrode while Ag/AgCl electrode was used as the reference electrode. The working electrolyte in all cases was 1 M H_2SO_4.

The observation made in the dark was that some hydrogen gas evolution occurs in both cases of the CdTe/steel and the plain stainless steel as working electrodes. Sunlight was simulated in the lab using a xenon lamp. In the light, there was noted an increase in current for the CdTe films compared to the dark, which was an indication that the fabricated films were photoactive.

For all the experiments, the sweep rate was maintained at 50 mV/s. In all the cases, there is evidence of oxidation and reduction peaks. Oxidation peaks are occurring above the horizontal axis while reduction peaks occur below the horizontal axis. When the voltage sweep was taken far to the negative, hydrogen ions (H^+) were being reduced and hydrogen gas bubbles were observed rising from the working electrode inside the electrolytic cell. When swept too far to the right, oxidation occurs. The following figures show the voltammograms for the fabricated CdTe films. All were performed in 1 M H_2SO_4, using Ag/AgCl reference electrode at 25 ^oC and a scan rate of 50 mV/s.

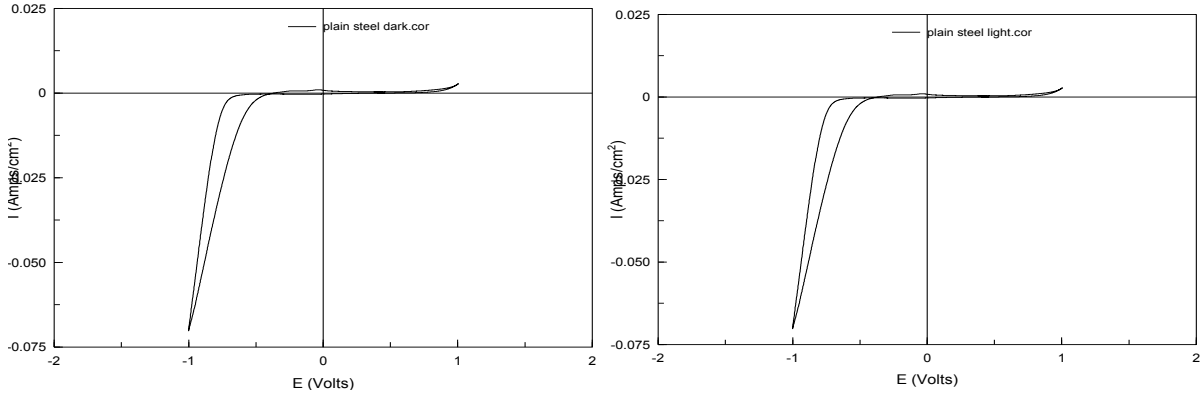

Figure 64: CV for plain steel in dark (left) and in light (right). Voltage sweep from 1.0 V to -1.0 V.

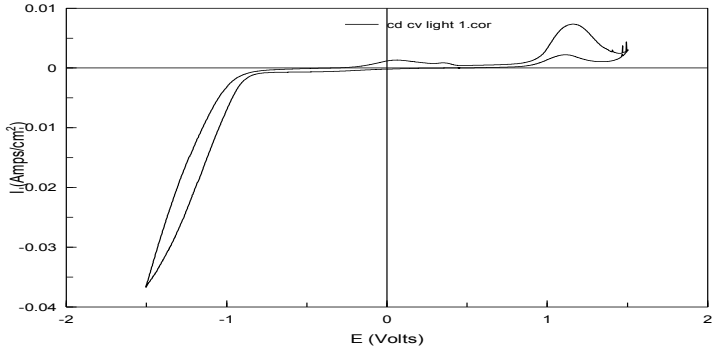

Figure 65: CV for a CdTe sample in light prepared at 300 ^{o}C. Voltage sweep from 1.5 V to -1.5 V.

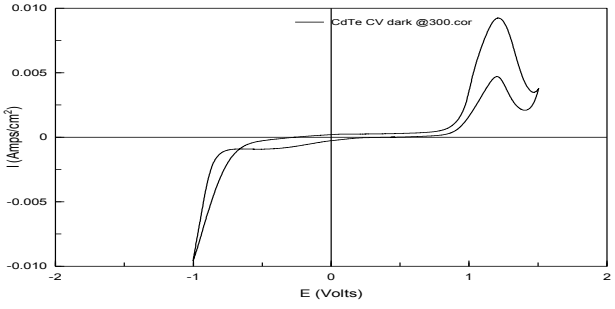

Figure 66: CV for a CdTe sample in dark, prepared at 300 ^{o}C. Voltage sweep from 1.5 V to -1.0 V.

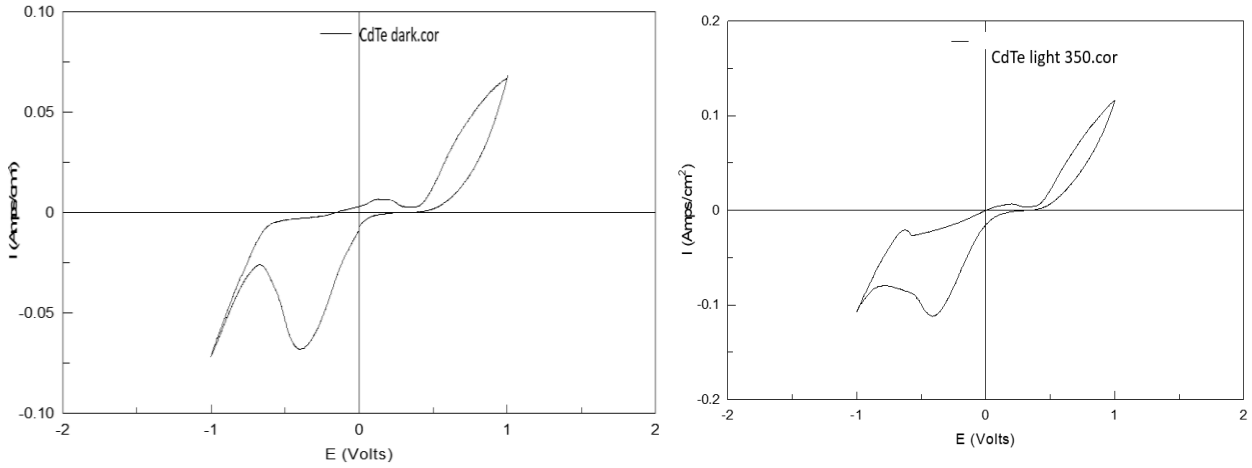

Figure 67: CV for CdTe films for the sample prepared at 350 ^{o}C for 5 minutes and annealed at 350 ^{o}C for 30 min.

As shown in Figures 65 - 67, there is evidence of oxidation where there is a peak observed above the horizontal axis and reduction observed from a peak below the horizontal axis. The oxidation peak may be due to the oxidation of the stainless-steel substrate. The reduction peak likely signifies the reduction of H^+ to make H_2 since the potential has been swept far negative of the thermodynamic potential as indicated by the Pourbaix diagram in Figure 13. At positive potentials, oxidation takes place generating oxygen from water. At the negative potentials, some hydrogen gas bubbles were observed in the electrolytic cell, implying the activity of the films. Linear sweep voltammetry (LSV) was done on the fabricated films. All LSV experiments were performed using 1M H_2SO_4 as the working electrolyte, Ag/AgCl as RE, and performed at 25 ^{o}C and a scan rate of 30 mV/s and various sweep voltage ranges. These LSV experiments were performed with the potential of the working electrode (WE) being varied while being kept constant at the RE. Figures 68 to Figure 72 below show the results for linear sweep voltammetry performed on the CdTe films.

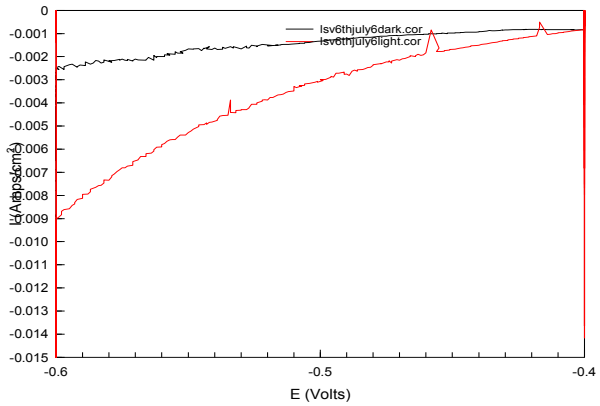

Figure 68: LSV for CdTe film fabricated at substrate temperature of 250 ºC and annealed at 350 ºC for 30 minutes. Photocurrent, 1780 µA/cm^2. Deposition time of 3 min. Voltage sweep from 0.0 V to -1.0 V.

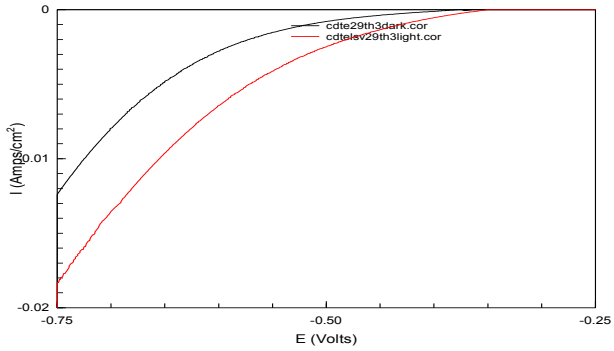

Figure 69: LSV for CdTe film fabricated at substrate temperature of 300 ºC and annealed at 350 ºC for 30 minutes. Photocurrent, 1698 µA/cm^2. Deposition time 3 min. Scan rate 30 mV/S. Voltage sweep from 0.0 V to -1.0 V.

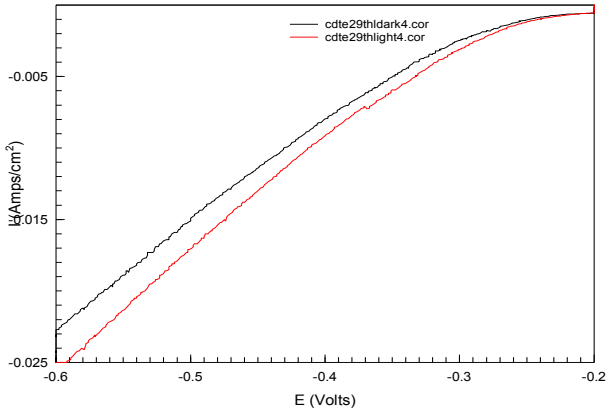

Figure 70: LSV for CdTe film fabricated at substrate temperature of 300 ºC and annealed at 350 ºC for 30 minutes. Photocurrent, 2000 µA/cm^2. Deposition time 5 min. Scan rate 30 mV/S. Voltage sweep from 0.0 V to -1.0 V.

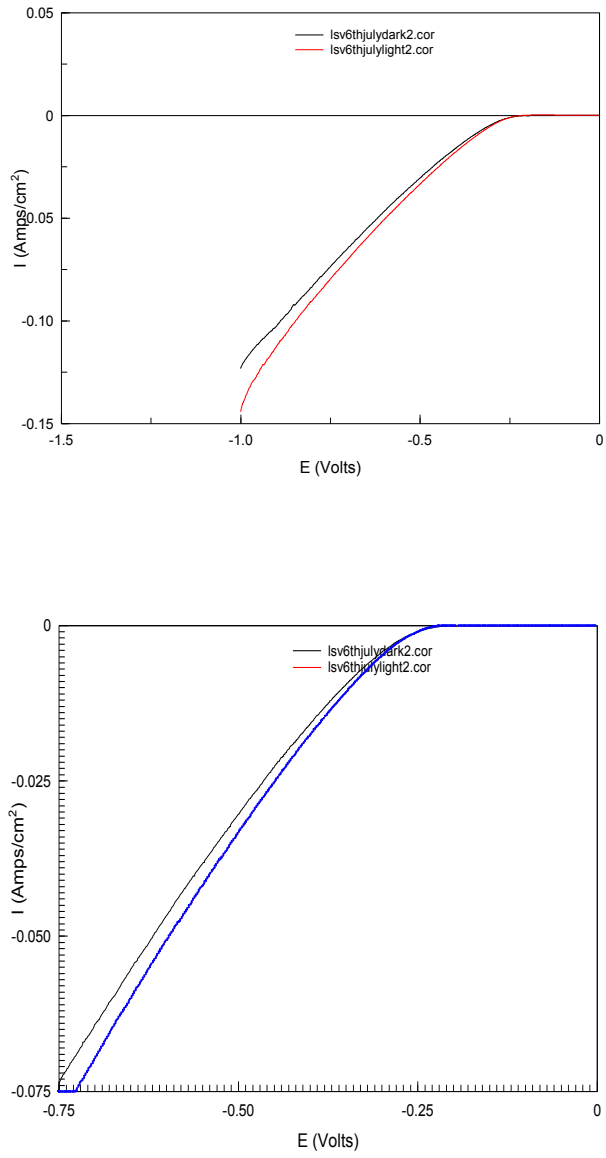

Figure 71: LSV for CdTe film fabricated at substrate temperature of 330 ^{o}C and annealed at 350 ^{o}C for 30 minutes. Photocurrent, 2900 µA/cm^2. Deposition time of 3 min. Scan rate 30 mV/S. Voltage sweep from 0.0 V to -1.0 V. The figure on top is the raw figure while the second shows the expanded figure to accurately read the axes.

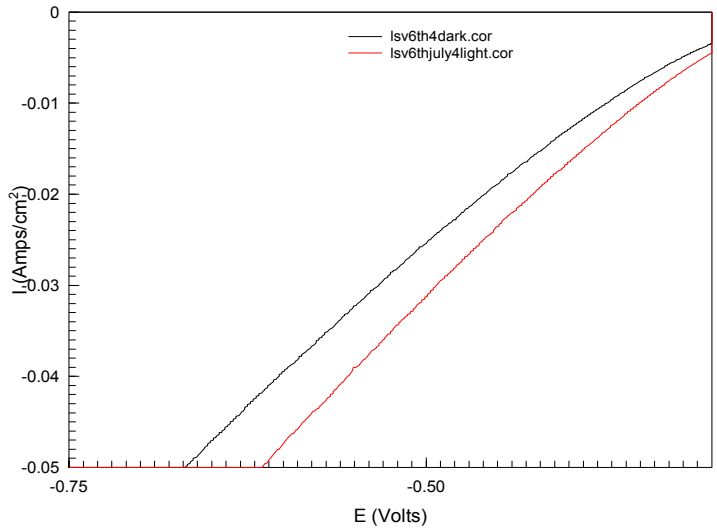

Figure 72: LSV for CdTe film fabricated at substrate temperature of 330 ºC and annealed at 350 ºC for 30 minutes. Photocurrent, 5800 µA/cm^2. Deposition time 5 min. Scan rate 30 mV/S. Voltage sweep from 0.0 V to -1.0 V.

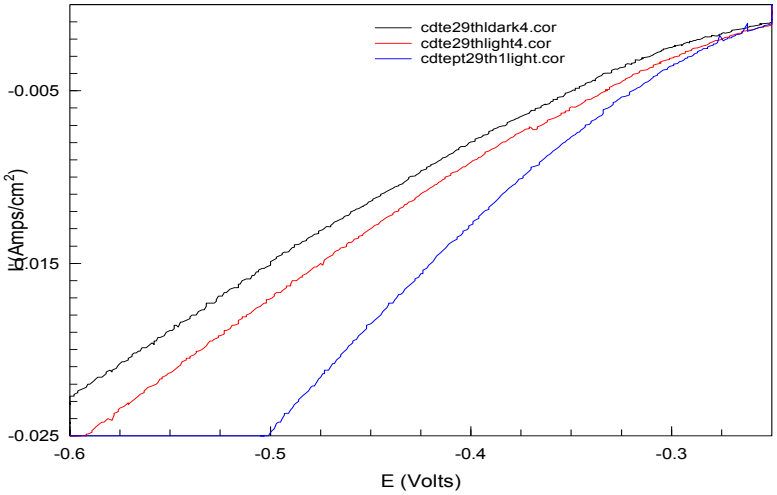

Figure 73: LSV for CdTe film fabricated at a substrate temperature of 300 ºC and performed in dark (black) and in light (red) and for platinized CdTe fabricated at 300 ºC and performed in light (blue). All were annealed at 350 ºC for 30 minutes. Photocurrent, 7700 µA/cm^2. Photocurrent enhanced by 5700 µA/cm^2.

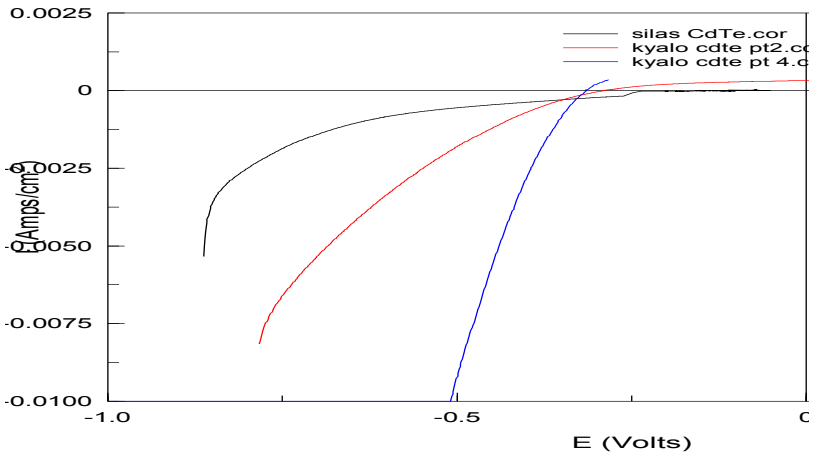

Figure 74: LSV for CdTe film fabricated at substrate temperature of 300 ºC and annealed at 350 ºC for 30 minutes in dark (black), for platinized CdTe in dark (red) and for platinized CdTe in light (blue). Deposition time 3 min. Scan rate 30 mV/S. Voltage sweep from 0.0 V to -1.0 V.

The LSV voltammetry for the films fabricated at different conditions showed some photocurrent. The measured photocurrent density ($\mu A/cm^2$) range was between 1698 $\mu A/cm^2$ and 7700 $\mu A/cm^2$. This was observed with the freshly fabricated and annealed CdTe films. Upon repeated exposure to 1 M H_2SO_4 and light for long time, the films were noted to get slightly etched, a phenomenon that needs to be studied further. The film fabricated at 250 ºC was the one mostly affected by this etching process with the film fabricated at 330 ºC being the least etched with equal exposure times. This observation could be related to the initial substrate temperature during the pyrolytic spray.

The platinized CdTe film (Figure 73) above showed an increase in photocurrent density by 1900 $\mu A/cm^2$ in light from the unplatinized counterpart. This shows that platinum by itself has a high potential for hydrogen evolution.

CHAPTER 5: CONCLUSION AND FUTURE WORK

5.1 Conclusion

In this project, CdTe thin films on SS 304 substrates were fabricated by use of the spray pyrolysis technique. The stainless-steel substrates temperature was varied during the spray and the quality of the resulting CdTe films was studied. The ideal substrate temperature for the spray pyrolysis of CdTe on SS-304 was found to be 300 ^{o}C – 350 ^{o}C with the optimum temperature at 330 ^{o}C, which produced well crystalline CdTe as observed from both XRD analysis and SEM-EDS analysis and had higher photocurrent. The fabricated films were observed to have a gray-to-black color, which is a characteristic color of CdTe. Annealing was important as noted since it improved the crystallinity of the CdTe and made the films very firm on the substrate and difficult to wipe off. Lowering the concentration of the precursor solutions from 0.02 M to 0.01 M led to a decrease in crystalline CdTe, requiring more time to produce a significant film. The film thickness determination was performed using the profilometry technique which showed that the thickness of the films based on a 3- to 5-minute spray trial was approximately 3 μm – 15 μm, implying a thin film on each substrate, which is the optimum range for CdTe operation. Powder XRD performed on the films revealed their crystalline structure, which was found to be cubic polycrystalline with the (111) plane being the preferred crystal orientation. SEM analysis done on the films revealed the morphology of the surfaces in which well-formed crystal boundaries were visible. EDS analysis gave details on the elemental composition of the films. The films mainly showed SS-304 substrate peaks and cadmium and tellurium elements. There was excess tellurium in the films compared to cadmium, implying a tellurium-rich surface which makes the semiconductor a p-type. CV performed on the films showed that the films were photoactive and that platinizing of the films catalyzes the process hence improving hydrogen gas generation.

5.2 Recommendation for future work

This project achieved a great step in showing the possibility of using the spray pyrolysis method of depositing CdTe on SS 304 for photoelectrochemical water splitting. However, we did not look at the possibility of using other metal substrates. As part of continued research on producing better photovoltaic films, we recommend the following: fabrication of CdTe thin films on other metal substrates other than SS 304, produce CdTe films by spray pyrolysis on steel and vary the spray conditions like the use of inert carrier gas instead of air. We also recommend that the effect of the concentration of the precursor solution to the quality of the fabricated films be studied further. In addition, we suggest a thermogravimetric analysis (TGA) be performed on the as-deposited CdTe films before annealing. We further propose that this spray pyrolysis of CdTe on SS 304 be considered in the mass production of the films over large surfaces. Finally, to improve electrical contact and practicality, we recommend a two-step deposition where CdTe is deposited by spray pyrolysis on a tellurium surface on SS 304 substrate and then an additional CdS layer.

REFERENCES

1. World energy and climate statistics- year book 2021. Retrieved from https://yearbook.enerdata.net/total-energy/world-consumption-statistics.html
2. Hannah, R.; Max, R.; Pablo, R.; (2022). - "Energy". Published online at OurWorldInData.org. Retrieved from: 'https://ourworldindata.org/energy'
3. Jun, L.; Xulei, Z.; Ting, M.; Lei Li, Shilin, W.; Meng, C.; Jijun, Z.; Haozhi, S.; Jian, H.; Yue S.; Linjun, W. Electrodeposition of CdTe Thin Films for Solar Energy Water Splitting. *Materials* 2020, 13, 1536; doi:10.3390/ma13071536
4. Https://www.un.org/en/climatechange/what-is-renewable-energy. Retrieved on 11/10/2022
5. Https://www.sun.org/encyclopedia/black-body-radiation. Retrieved on 11/10/2022
6. Anaa, L. (2020). Advantages of solar energy and why switch to solar panels. Retrieved from: https://Linguip.com/blog/advantages-of-solar-energy/. Retrieved on 01/14/2023
7. Kasper T., Torben R. J., Etsuo A., Hai-wen L. Hydrogen - A sustainable energy carrier. *Progress in Natural Science: Materials International,* 27(2017) 34-40.
8. Https://solenergy.com.ph/solar-panel-philippines-edmond-becquerel/
9. Solar power authority staff (2023) A History of Solar Cells: How Technology Has Evolved https://www.solarpowerauthority.com/a-history-of-solar-cells/
10. Chopra, K; Paulson, D.; Dutta, V. Thin-Film Solar Cells: An Overview. Progress in photovoltaics: Research and applications Prog. Photovolt: Res. Appl. 2004; 12:69–92 (DOI: 10.1002/pip.541)
11. Byju's, (2023). Fermi Energy. Retrieved from https://byjus.com/physics/fermi-energy/. Retrieved on 02/01/2023
12. Https://eng.libretexts.org/Bookshelves/Materials_Science/Supplemental_Modules_(Materials_Science)/Solar_Basics/C._Semiconductors_and_Solar_Interactions/I._Basic_Properties_of_Semiconductors/4._Fermi_Energy_Levels. Retrieved on 02/01/2023
13. Nithyayini, K.N; Ramasesha, S.K. (2015). Fabrication of Semi-Transparent Photovoltaic Cell by a Cost-Effective Technique. *ASM International (ASM) and The Minerals, Metals & Materials Society (TMS)*. DOI: 10.1007/s40553-015-0053-x.
14. Xin, L.; Jiaguo, Y.; Jingxiang, L.; Yueping, F.; Jing, X.; and Xiaobo, C. Engineering heterogeneous semiconductors for solar water splitting. *J. Mater. Chem. A*, 2015, 3, 2485-2534

15. Michelle Fung (2005). Energy density of hydrogen. The Physics factbook. Retrieved from, https://hypertextbook.com/facts/2005/MichelleFung.shtml
16. Atiqur, R. (2022). Why it's crucial to understand the fill factor of solar cell? How it's affecting the efficiency of PV cells?
17. Polycrystalline silicon *Wikipedia* 2022, December 22. Https://en.wikipedia.org/wiki/Polycrystalline_silicon. Retrieved on 01/15/2023
18. Https://www.linquip.com/blog/what-is-a-monocrystalline-solar-panel/. Retrieved on 02/08/2023
19. Gunjal, S.D.; Khollam, Y.B.; Jadkar, S.R; Shripathi, T.; Sathe, V.G.; Shelke, P.N.; Takwale, M.G.; Mohite, K.C. Spray pyrolysis deposition of p-CdTe films: Structural, optical and electrical properties. Solar energy 106 (2014) 56-62
20. Shockley–Queisser Limit, Theoretical Maximum solar cell efficiency. From; https://solaredition.com/wp-content/uploads/2019/03/shockley–queisser-limit-theoretical-maximum-solar-cell-efficiency. -in-science-the-shockley–queis.jpg. Retrieved on 03/10/2022
21. Https://www.linquip.com/blog/monocrystalline-vs-polycrystalline/. Retrieved on 01/13/2023
22. Https://eng.libretexts.org/Bookshelves/Materials_Science/Supplemental_Modules_(Materials_Science)/Solar_Basics/C._Semiconductors_and_Solar_Interactions/I._Basic_Properties_of_Semiconductors/4._Fermi_Energy_Levels. Retrieved on 01/19/2023
23. Ubale, A.; Dhokne, R.; Chikhlikar, P.; Sangawar, V.; Kulkarni, D. (2006). Characterization of nanocrystalline cadmium telluride thin films grown by successive ionic layer adsorption and reaction (SILAR) method. *Bull. Mater. Sci*., Vol. 29, No. 2, pp. 165–168.
24. Steven K. (2022). What are Cadmium Telluride (CdTe) Solar Panels? How Do They Compare to Other Panels? Retrieved from https://solarbuy.com/solar-101/cdte-cadmium-telluride-solar-panels/. Retrieved on 02/01/2023
25. Harper, Gavin, D.J. "cadmium telluride solar cell". *Encyclopedia Britannica*, 21 Dec. 2015, https://www.britannica.com/technology/cadmium-telluride-solar-cell. Accessed 1 February 2023.
26. Shaikh, S.S.; Mohd, S.; Masumdar, E.U., (2020). Exploration of the spray deposited Cadmium Telluride thin films for optoelectronic devices. *Physica B: Physics of Condensed Matter*, 580 (411831), 1-8.

27. Poplawsky, J. Cadmium telluride solar cells: Record-breaking voltages. *Nat Energy* **1**, 16021 (2016). https://doi.org/10.1038/nenergy.2016.21
28. Gunjal, S.; Khollam, Y.; Jadkar, S.; Shripathi, S.; Sathe, V.; Shelke, P.; Takwale, M.; Mohite, K. Spray pyrolysis deposition of p-CdTe films: Structural, optical and electrical properties. *Solar energy* 106 (2014) 56-62
29. Tembhurkar, Y.D. (2016). Electrical Properties of Solid-Solution II-VI of CdTe Thin Films Prepared by Spray Pyrolysis. *IOSR Journal of Applied Physics (IOSR-JAP)*, 8(6), 50-51.
30. Krishna, K.V.; Dutta, V. Spray deposition of CdTe–Te thin films using ethylene-diamine-tetra-acetic acid as a complexing agent in the precursor solution. *Solar Energy Materials & Solar Cells* 80 (2003) 247–256.
31. Tembhurkar, Y.D. (2015). Temperature Dependence of Electrical Properties and Thickness of II-VI Solid-Solution of CdTe Thin Films Prepared by Spray Pyrolysis. *International Journal of Science and Research (IJSR)*, 5(12), 1293-1294
32. Dainius, P.; Ludwig, J. G. (2005). Thin Film Deposition Using Spray Pyrolysis. *Journal of Electroceramics*, 14, 103–111.
33. Jingwang, Lian, G. (2018). Metal oxide semiconductors for water solar splitting. Retrieved from, sciencedirect.com/topics/engineering/water-splitting#. Retrieved on 04/02/2022
34. Xin, L.; Jiaguo. Y.; Jingxiang, L.; Yueping, F.; Jing, X.; Xiaobo, C. Engineering heterogeneous semiconductors for solar water splitting. *J. Mater. Chem. A*, 2015, 3, 2485-2534
35. Stephen, R.; Mettee, H.; Linkous, C. (2012). Development of a hydrogen-evolving photocatalytic membrane. *Energy Procedia*, 29, 522-531.
36. Advanced nano-structured materials for photocatalytic water splitting. *Journal of Electrochemical Science and Technology* 2016;7(1):
37. Samanta, S.; Shinde, M. S.; Dipak, S.; Patil, R.S. Studies on growth and characterization of CdTe thin films deposited by chemical bath deposition technique. *Applied Science Research*, 2015, 7 (11), 10-15.
38. Hankare, P.P.; Rathod, K.C.; Asabe, M.R.; Jadhav, A.V.; Garadkar, K.M. Preparation and characterization of cadmium telluride thin films by chemical bath deposition method. *MSAIJ*, 4(1), 2008 [28-32].

39. Naser, A.; Joao, A.; Teixeira; Abdulmajid, A.; Maryam, S.; Feras, A.; Ahmad, S.; Husain, B. (2019). Deposition of Stainless-Steel Thin Films: An Electron Beam Physical Vapour Deposition Approach.
40. Murase & Kuniaki. (1999). Potential-pH Diagram of the Cd-Te-NH[sub 3]-H[sub 2]O System and Electrodeposition Behavior of CdTe from Ammoniacal Alkaline Baths. *Journal of The Electrochemical Society - J ELECTROCHEM SOC*. 146. 10.1149/1.1391846.
41. Dainius, P.; Ludwig, J. G. (2005). Thin Film Deposition Using Spray Pyrolysis. *Journal of Electroceramics*, 14, 103–111.
42. Pramod, S. P. Versatility of chemical spray pyrolysis technique. *Materials Chemistry and Physics*, 59 (1999) 185-198.
43. S.S. Shaikh, Mohd Shkir, E.U. Masumdar (2020). Exploration of the spray deposited Cadmium Telluride thin films for optoelectronic devices. *Physica B: Physics of Condensed Matter*, 580 (411831), 1-8.
44. Rutto, P. (2018). Electrodeposition of CdTe on the Stainless Steel 304 substrates. *Student thesis paper*. Youngstown State University, Ohio.
45. Malika, J. (2021). Electroless Deposition of CdTe on Stainless Steel 304 Substrates. *Student thesis paper*. Youngstown State University, Ohio.
46. Alonzo-Medina, G.M., (2013). IOP Conf. Ser.: *Mater. Sci. Eng*. 45 012013
47. Dutrow, B.; Clark, M.C. X-ray powder diffraction (XRD). Geochemical instrumentation and analysis. Louisiana State University. Retrieved from https://serc.carleton.edu/research_education/geochemsheets/techniques/XRD.html. Retrieved on 02/09/2023.
48. Editorial board (2022). Scanning electron microscope (SEM). Microscopewiki. Retrieved from https://microscopewiki.com/scanning-electron-microscope/. Retrieved on 02/03/2023
49. Elgrishi, N.; Rountree, K.J; McCarthy, B.D; Rountree, E.S; Eisenhart, T.T.; Dempsey, J.L. *A Practical Beginner's Guide to Cyclic Voltammetry* J. Chem. Educ., vol. 95, no. 2, pp. 197–206, 2018
50. Haus, J.W., (2016). Fundamentals and applications of nanophotonics. Surface profiling. https://doi.org/10.1016/B978-1-78242-464-2.00006-3. Retrieved on 02/03/2023.